Farkas, M. P., Yoon, J.-S., Zang, A., Zimmermann, G., Stephansson, O., Lemon, M., Dankó, G. (2019): Effect of Foliation and Fluid Viscosity on Hydraulic Fracturing Tests in Mica Schists Investigated Using Distinct Element Modeling and Field Data. - *Rock Mechanics and Rock Engineering*, *52*, 2, pp. 555—574.

DOI: http://doi.org/10.1007/s00603-018-1598-7

Effect of foliation and fluid viscosity on hydraulic fracturing tests in mica schists investigated using distinct element modeling and field data

Márton Pál Farkas[a,b,c], Jeoung Seok Yoon[d], Arno Zang[d,c], Günter Zimmermann[a], Ove Stephansson[d], Michael Lemon[e] and Gyula Dankó[b]

[a] Section 6.2 Geothermal Energy Systems, GFZ - German Research Centre for Geosciences, Telegrafenberg, Potsdam 14473, Germany

[b] Golder Associates Hungary, Hűvösvölgyi út 54, Budapest 1021, Hungary

[c] Institute of Earth and Environmental Science, University of Potsdam, Karl-Liebknecht-Straße 24/25, Potsdam 14476, Germany

[d] Section 2.6 Seismic Hazard and Risk Dynamics, GFZ - German Research Centre for Geosciences, Telegrafenberg, Potsdam 14473, Germany

[e] Golder Associates Ltd., 6925 Century Avenue, Suite 100, Missisouga, Ontario L5N 7K2, Canada

Abstract

Several hydraulic fracturing tests were performed in boreholes located in central Hungary in order to determine the in-situ stress for a geological site investigation. At a depth of about 540 meters, the observed pressure versus time curves in mica schist with low dip angle foliation show atypical pressure versus time results. After each pressurization cycle, the fracture breakdown pressure in the first fracturing cycle is lower than the refracturing or reopening pressure in the subsequent pressurizations. It is assumed that the viscosity of the drilling mud and observed foliation of the mica schist have a significant influence on the pressure values. In order to study this problem, numerical modelling was performed using the distinct element code PFC (Particle Flow Code), which has been proven to be a valuable tool to investigate rock engineering problems such as hydraulic fracturing. The two-dimensional version of the code applied in this study can simulate hydro-mechanically coupled fluid flow in crystalline rock with low porosity and pre-existing fractures. In this study, the effect of foliation angle and fluid viscosity on the peak pressure is tested. The atypical characteristics of the pressure behavior are interpreted so that mud with higher viscosity penetrates the sub-horizontal foliation plane, blocks the plane of weakness and makes the partly opened fracture tight and increase the pore pressure which decreases slowly with time. We see this viscous blocking effect as one explanation for the observed increase in fracture reopening pressure in subsequent pressurization cycles.

Keywords: Hydraulic fracturing; Stress measurement; Particle Flow Code; Hydro-mechanical coupling; Micro cracking; Viscous blocking

* Corresponding author. Tel.: +49 331 288 1898

E-mail address: farkas@gfz-potsdam.de

List of symbols

HF	Hydraulic Fracturing
LOT	Leak-off Test
xLOT	Extended Leak-off Test
FBP	Fracture breakdown pressure
NPP	Nuclear power plant
RFP	Refracturing pressure or reopening pressure
SIP	Shut-in pressure
ISIP	Instantaneous shut-in pressure
DPDT	Derivative shut-in pressure
JP	Jacking pressure
P_f	Fluid pressure
σ_3	Minimum principal stress
σ_1	Maximum principal stress
σ_n	Normal stress
S_v	Vertical stress
S_{hmin}	Minimum horizontal stress
S_{Hmax}	Maximum horizontal stress
S_{xx}	Stress parallel to axis x
S_{zz}	Stress parallel to axis z
UCS	Uniaxial Compressive Strength
BTS	Brazilian Tensile Strength
T	Tensile strength of the rock
Q	Flow rate
e	Hydraulic aperture
e_0	Hydraulic aperture at zero normal stress
e_{inf}	Hydraulic aperture at infinite normal stress

α	Coefficient of decay
η	Dynamic fluid viscosity
R	Particle radius
m	Particle mass
a	Acceleration
K_c	Contact stiffness
K_b	Bond stiffness
U	Particle overlap
V_{inj}	Injected fluid volume

1. Introduction

The knowledge of the current stress state is essential for underground construction and stability. To determine the in situ state of stress at a given site is a challenging task (Stephansson and Zang 2012). In particular, stress magnitudes play a key role in calibration of geomechanical models for the safety assessment of underground or surface site such as nuclear waste repository or nuclear power plant (*NPP*). The measured in-situ stress field contributes to the assessment of tectonic evolution and any potential fault slip. A fault slip may jeopardize the long term stability of the facilities. Therefore, such assessments must consider the ranges of stress magnitudes and orientation at different depths to determine tectonic regimes and their stability.

Hydraulic fracturing (*HF*) is the most widely used in-situ stress measurement technique that enables estimating stress magnitudes and orientation at various depths over relatively large rock volume, i.e. 0.5 to 50 m^3 (Amadei and Stephansson 1997). The suggested *HF* test procedure by Haimson and Cornet (2003) and Zang and Stephansson (2010) is summarized as follows.

The suggested method assumes a borehole drilled parallel to a principal stress direction (typically vertical) and requires the identification of rock formations to be tested using extracted cores and/or borehole images. The selection of test intervals for *HF* aims at avoiding fractures or other structural features. The test interval is sealed off by inflating straddle packers at the selected depth, generally by pumping water.

The test interval is first pressurized to assess the performance of the packers and to confirm that open, conductive fractures are not present (formation integrity test). During the first, breakdown cycle, the interval pressure is raised by maintaining a constant, predetermined, flow rate to achieve the peak pressure at which the borehole wall

fractures, termed as fracture breakdown pressure *FBP* (Zang and Stephansson 2010) within 3 to 5 minutes. Immediately after observing tensile breakdown, the interval pressure is shut-in to limit the extent of hydraulic fracture propagation. Interval pressure will decay, initially at a higher rate while the newly created hydraulic fracture is still open, and then much slower, after the fracture has closed. The pressure decay is monitored for approximately 5 minutes, then released to initial, static pressure (termed as venting or flow back). The pressure at which the fracture closes is termed shut-in pressure (*SIP*). The pressure measured immediately after the shut-in operation started is referred to as instantaneous shut-in pressure (*ISIP*).

Once the interval pressure returns to the static pressure, the interval is pressurized at the same flow rate as breakdown cycle to observe the reopening or refracturing pressure of the newly created hydraulic fracture (*RFP*). The flow is maintained for several minutes to observe the fracture propagation pressure, followed by shut-in. The pressure decay is monitored to identify the shut-in pressure. Reopening cycles can be conducted two or three times in order to establish consistent fracture reopening and shut-in pressure.

After the reopening cycle(s), a step-rate or jacking pressurization cycle can be conducted to confirm the RFP under controlled conditions. The pressure in the interval is first brought to a very low level and maintained constant while the flow rate is measured. Thereafter, the interval pressure is raised to a new higher value and again the flow rate is allowed to stabilize at a constant level. This is repeated several times, which results in constant pressure levels measured at different flow rates. Once the interval pressure exceeds the RFP, the newly created fracture opens, i.e. deviation from linear trend is observed on pressure versus flow rate plot. The injection is stopped and the test interval is shut-in for pressure decay monitoring. After completion of the test cycles, the packers are deflated and moved to the next test interval.

The fluid pressure required to generate, propagate, sustain and reopen fractures in rock is related to the magnitude of the existing stresses. The direction of the in-situ stresses is inferred by observing the orientation of the hydraulically induced fractures by comparison of the pre- and post-test (acoustic or resistivity) borehole images to determine the presence and orientation of a newly created hydraulic fracture.

Although it is relatively straightforward to measure stress magnitudes using *HF* (Zang and Stephansson 2010, Zoback 2010), pressures determined by this method still suffers from uncertainties due to the natural (intrinsic) anisotropy and heterogeneity of the rock mass. Furthermore, uncertainties in *HF* stress measurements are not only

related to inherent rock properties but also to measurement technique and data analysis (Amadei and Stephansson 1997).

It must be noted that methods commonly used for determining the minimum stress – apart from traditional hydraulic fracturing – are the leak-off tests (*LOT*) and extended leak-off tests (*xLOT*). The main difference between *HF* and *LOT*/*xLOT* is that *HF* is conducted in a section away from the well bottom while the latter is normally performed under the casing shoe, typically at the very bottom of the drill hole. The difference in geometry between *HF* and *LOT*/*xLOT* is likely to have an influence on the determination of the minimum stress (Zang et al. 2012).

Several field, laboratory and numerical studies have been reported on pressure-time records that are unusual and make the interpretation complicated. In the following, we give three examples for anomalous breakdown and peak pressure behavior during HF testing. First, early in-situ *HF* tests in deep intervals (up to 1000 m depth) as reported by Healy and Zoback (1988) and Hickman and Zoback (1983) show the peak pressure attained in crystalline rock on the first cycle is lower than that attained on subsequent cycles. The authors explain the unusual behavior by either fracture formation at the time of the packer inflation or low, and varying rock tensile strength. Second, recent HF stress measurements in granite and shale on laboratory scale reported by L. Zhou et al. (2016) and Lin et al. (2017), respectively, show similar, peak pressure features when increasing injection fluid density and viscosity. These observations from laboratory investigations are also supported by results from numerical modeling presented by Shimizu et al. (2011) and Zhou J et al. (2016a).

In this study, we use recent in-situ *HF* rock stress measurements in boreholes at depth up to 1500 m that were conducted by Golder Associates Hungary (Lemon et al., 2016) to assess the stress regime as part of a geotechnical and hydrogeological investigation for the Paks II Nuclear Power Plant (*NPP*) Extension Project (Paks II project) in Hungary (ÁKMI, 2016). At several test intervals, in-situ *HF* stress measurements were performed in which recorded pressure – time data exhibit higher *RFP*s than *FBP*.

The goal of this study is to better understand processes that can lead to larger reopening fracture pressure *(RFP)* than first breakdown pressure (*FBP)* as observed in stress measurement data obtained in the project. Thus, we performed numerical modelling using the distinct element method and the two-dimensional Particle Flow Code, PFC^{2D} (Itasca, 2008) to simulate several pumping cycles in three different PFC models.

The paper is structured as follows. In section 2, the most relevant characteristics of the Paks II *NPP* Extension Project and the *HF* rock stress field measurements are summarized. In section 3, the two-dimensional hydro-

mechanically coupled discrete element code and the model geometry are reported. In section 4, the injection procedure and the breakdown and reopening pressure cycles are described. In section 5, results of the PFC modeling are compared with field data, assessed and discussed. Finally, the viscous blocking idea is developed for anisotropic rock (mica schist) to explain the lowering of peak pressure in subsequent hydraulic testing cycles observed in the field.

2. Hydraulic Fracturing Stress Measurements and Data

2.1 The Paks II Project Testing Program

The Paks Nuclear Power Plant (*NPP*) is located south of the town of Paks in central Hungary (Fig. 1). To comply with requirements of the Hungarian Atomic Energy Authority and the International Atomic Energy Agency for permitting construction of new power units, referred to as Paks II project, a geological investigation was conducted in 2015-2016 (ÁKMI 2016). In the framework of this project, several Hydraulic Fracturing (*HF*) stress measurements were performed to create a geomechanical model of the site (Lemon et al., 2016). The measurements were conducted at 19 intervals in each of four boreholes, PAET-26, PAET-27, PAET-29 and PAET-34, drilled for geotechnical and hydrogeological investigations. Figure 1 shows the location of the four boreholes tested and Fig. 2 summarizes the obtained stresses. The target depths of the test zones were selected to assess the in-situ stresses within the primary geologic units of the site. Variscan metamorphic basement rocks are intercepted by borehole PAET-26, Mesozoic carbonate basement rocks (Jurassic marl and limestone rocks) are intercepted by borehole PAET-27 and Miocene dacitic rocks (Mecsek Andesite Formation) intercepted by PAET-29 and PAET-34. The depth of test intervals varies between 500 and 1500 m.

The testing equipment was provided by Golder Associates Hungary and included the following:

- Two inflatable packers, arranged for a test interval length of 1.33 meters;
- High pressure pump for inflating packers and injecting water into the test interval;
- Inflation line attached to the test tubing;
- Flow control board, located at surface for controlling water pressure and flow rate of test interval and packer pressure;
- Electronic instrumentation and data acquisition system for monitoring and recording injection pressures, flow rates and packer pressures; and

- Pressure gauge with internal memory, positioned inside the test interval.

Packer pressure, test interval pressure, and flow rate were continuously monitored and recorded during each test. Pre- and post-testing acoustic borehole images (BHTV) were used to determine the location and orientation of any newly created fracture.

2.2 Results of Hydraulic Fracturing Tests in Borehole PAET-26

In this paper, we focus on the interpretation of the pressure versus time records of the test results from borehole PAET-26 as a representation of the test intervals showing ambiguities in the interpreted *FBP* and *RFP*. For other test interval results and analysis, the reader is referred to ÁKMI (2016) and Lemon et al. (2016).

Borehole PAET-26 was drilled vertically down to 560 m, with a 4 ¾" casing down to 502 m in 2015. The tested open hole section is approx. 60 m long with a diameter of 96 mm. The open hole section is located in Variscan metamorphic basement rock formation which lies beneath the poorly consolidated sedimentary sequence of Upper Pannonian Újfalu and Algyő Formations (Fig. 3).

In borehole PAET-26, the rock tested is fresh, strong, dark gray to light gray, mica schist which has a W-NW strike and mostly shallow dipping foliation of between 0° and 15° at depth between 500 to 550 m (Fig. 4). Test intervals in crystalline basement rock were selected from sections free of natural fractures and relatively limited presence of planes of foliation planes. Prior to testing, the open borehole intervals were not flushed by water to prevent wellbore instabilities. Thus, hydraulic fracturing could only be performed using drilling mud with a density of 1060–1160 kg/m^3.

The goal of the pressurization cycles is to provide sufficient data to obtain repeatable values of the following pressures from each test interval:

- Fracture breakdown pressure (*FBP*), determined from the peak pressure of Cycle 1;
- Reopening or refracturing pressure (*RFP*), identified as the variation in pressurization rate of Cycle 2 relative to Cycle 1;
- Derivative shut-in pressure (*DPDT*), determined by the intersection of tangents on the time derivative of pressure plot, which indicate a change in the interval conductivity caused by the fracture closure, from cycle 2 and subsequent cycles; and

- Jacking pressure (*JP*), determined by the deviation from linear or laminar flow on the plot of pressure against flow rate from a series of jacking or step-rate test steps based on Doe and Korbin (1987).

These pressure values are used to estimate the minimum stress (σ_3) exerted perpendicular to the fracture face that is opened. The maximum horizontal stress (S_{Hmax}) is calculated from the minimum horizontal stress (S_{hmin}), the *FBP*, the *RFP*s and the tensile strength of the rock (*T*) using the Hubbert-Willis equation in Zang and Stephansson (2010):

$$S_{Hmax} = 3S_{hmin} - FBP + T - P_p, \quad (1)$$

where P_p is the pore pressure. The vertical stress, the magnitude of overburden load or lithostatic stress (S_v) is accepted to act vertically, parallel to the well orientation, and is calculated from the cumulative neutron density profile.

Three successful *HF* tests were completed in PAET-26. The complete pressure-time records for one of the tested intervals in PAET-26 for depth at 540.33 to 541.66 m are presented in Fig. 5a as a representation of all conducted measurements in this borehole. The breakdown, refracturing, shut-in and jacking pressures and the estimated stresses for this interval are calculated, and summarized in Table 1. These show that after an initial interval or formation integrity test (*FIT*), a breakdown cycle is followed by two refracturing cycles and a jacking cycle. The jacking cycle was invalid due to pump malfunction. A third refracturing cycle was conducted with an extended pumping period followed by a modified jacking cycle and a final, fourth refracturing cycle.

The interval tested shows a tensile *FBP* in Cycle 1 with increasing peak pressures in subsequent refracturing cycles to a maximum of 19.3 MPa in Cycle 3 at a flowrate of approximately 4 l/min (Fig. 5b). The shut-in pressure (*SIP*) of the refracturing cycles as well as the jacking cycle show similar fracture closure pressure of approximately 16.4 MPa. The determination of fracture closure pressure from cycle 2 using the pressure versus square root time and DPDT plots is illustrated in Fig. 6a and Fig. 6b, respectively.

Based on these consistent pressures, the minimum principal stress of 16.4 MPa is selected for the test interval. Using eq. (1), the estimated maximum principal stress (σ_1) equals 29 MPa. The vertical stress (S_v) is estimated as 11.6 MPa from neutron density logging. Figure 2 shows that the minimum stresses measured for all three tests in this well are above lithostatic stress, which indicates either thrust faulting regime ($S_v < S_{hmin} < S_{Hmax}$) or the test results indicate an intermediate stress (Table 1 and Fig. 2).

Comparison of pre and post-testing acoustic televiewer logs for three tested intervals in PAET-26 does not show any newly induced hydraulic fracture (Fig. 4), which prohibits assessment of the direction of the measured minimum stress.

The estimated stresses and the lack of presence of induced hydraulic fracture in the post-testing borehole image imply that either the fracture closed completely after *HF* or the newly induced or reactivated fracture propagated in the direction of the sub-horizontal foliation plane.

Fig. 1 Map of Pre-Cenozoic basement rock in central Hungary, showing mapped faults. The boundary of the study area of Paks II project is indicated by black square (60 x 60 km). The map shows the location of boreholes tested excluding PAET-30 (yellow circles). The Paks Nuclear Power Plant is indicated by green triangle. Rock types: Cyan (color code 10): Lower-middle Jurassic pelagic, fine siliciclastic rock; pink (color code 23): Variscan metamorphic rock (after ÁKMI 2016)

Fig. 2 Summary of in-situ stresses measured at 19 intervals in basement rock of boreholes PAET-26, PAET-27, PAET-29 and PAET-34 for the Geological Research Program for Paks II project in Hungary (after Lemon et al. 2016)

Fig. 3 Stratigraphy and well construction diagram of borehole PAET-26

Fig. 4 Pre- and post-testing acoustic borehole televiewer (BHTV) logs of the tested Mica Schist rock interval in borehole PAET-26 at approx. 540 m depth. Area highlighted in green in center shows the hydrofractured interval which does not show any fracture prior to testing. The areas in black below and above the interval show the location of the straddle packers. Continuous, blurry areas are results of device effects. No new features are visible in the post-testing images which indicates an induced fracture that closed after stimulation or hydraulic fracture propagation in horizontal plane. For color interpretation of this figure, the reader is referred to electronic version of this paper (after Lemon et al. 2016)

Fig. 5a Summary plot of interval pressure and flow rate of pressurization cycles at a tested interval at approximately 540 m depth in borehole PAET-26. The cycles are indicated by numbers with respect to information in Table 1. Black thick and thin pressure curves show pressure recorded at the interval and within the packers, respectively. Vertical lines indicate the duration of each injection cycle. Flow rate (blue) during injection and flow back are plotted on same positive axis. For color interpretation of this figure, the reader is referred to electronic version of this paper (after Lemon et al. 2016)

Fig. 5b Summary plot of interval pressure and flow rate of pressurization cycle 1 (Breakdown) and cycle 2 (Refracturing) at a tested interval at approximately 540 m depth in borehole PAET-26. Black thick and thin pressure curves show pressure recorded at the interval and within the packers, respectively. Thick and dashed vertical lines indicate duration of each cycle and operations during testing, respectively. Flow rate (blue) during injection and flow back are plotted on same positive axis. For color interpretation of this figure, the reader is referred to electronic version of this paper (after Lemon et al., 2016)

Fig. 6a Plot of pressure versus square root time showing a *SIP* of 16.4 MPa for cycle 2 (Refracturing) at a tested interval at approximately 540 m depth in borehole PAET-26 (after Lemon et al. 2016)

Fig. 6b Time derivative of pressure (*DPDT*) versus square root time showing a *SIP* of 16.4 MPa for cycle 2 (Refracturing) at a tested interval at approximately 540 m depth in borehole PAET-26 (after Lemon et al. 2016)

Table 1 Summary of *HF* tests in one tested intervals as a representation for all three in-situ stress measurements in borehole PAET-26. Pressures presented are measured at the test interval, which includes the pore pressure. The pressures in bold provide confidence in the selected minimum stress (S_{hmin}) value (after Lemon et al., 2016)

3. Numerical Model

3.1. Two-dimensional Particle Flow Code and fluid flow algorithm

The ITASCA Particle Flow Code (PFC^{2D}) uses an explicit time integration scheme to solve the equations of motion for an aggregate of rigid discrete circular particles (Itasca 2008). PFC^{2D} is also referred to as the bonded-particle model (BPM) since the contacts between the circular particles are defined through so-called parallel bonds and enhanced by cementing material at the contacts with finite thickness (Fig. 7). The integration scheme, that is, the mechanical calculation cycle in PFC2D is a time stepping algorithm that iterates between the law of motion applied to each particle and the linear force displacement law including fluid induced deformation applied to each contact (Fig. 8). The geomechanical simulator defines strength at the contacts in terms of Mohr-Coulomb failure criterion (Itasca 2012; Labuz and Zang 2012). Due to mechanical loading and loading from fluid pressure, the bonds can break in tension (Mode I) or shear (Mode II). For more details, we refer to Potyondy and Cundall (2004).

The fluid flow algorithm of the hydraulic cycle provides a way to investigate hydraulic treatment from a borehole into the host rock. In this study we use the hydro-mechanically coupled code of PFC^{2D} developed by Hazzard (2002), Yoon et al. (2014) and Yoon et al. (2017). The algorithm assumes that each particle bonded contact corresponds to a flow channel which connects up pore spaces (so-called domains) that can store pressure and once a domain is pressurized, it becomes fully saturated (Fig. 7). In this sense poroelasticity is explicitly considered in the applied version of PFC^{2D}.

We use the experimentally derived relation between hydraulic aperture and normal stress in crystalline rock based on Hökmark et al. (2010):

$$e = e_{inf} + \left(e_0 - e_{inf}\right) exp(-\alpha\sigma_n), \tag{2}$$

where e_{inf} denotes the residual hydraulic aperture at infinite normal stress, e_0 is hydraulic aperture at zero normal stress, σ_n corresponds to effective normal stress on a flow channel and coefficient α controls the rate of aperture decrease with increasing normal stress. We assume that the foliation plane does not have asperities that may prevent surface closure. Based on developments by Yoon et al. (2017) the PFC^{2D} code uses two different hydraulic

aperture (e) versus normal stress (σ_n) relations. These are assigned to particle contacts representing foliation (smooth joint introduced by Mas Ivars et al. 2008) and rock matrix (parallel bond). Figure 9 shows that initial hydraulic aperture (e_0) in rock matrix (orange) is approx. 0.6 µm and 6 µm in foliation (blue) and decreases to 0.1 µm and 1 µm (e_{inf}), respectively, with increasing normal stress. These values are in good agreement with aperture derived from field hydraulic tests (ÁKMI 2016). Coefficient of decay (α) is set to 0.15 for both foliation and rock matrix based on Hökmark et al. (2010).

Permeability of rock matrix and foliation are defined by hydraulic aperture. The initial hydraulic aperture for a given permeability (k) is estimated using the derivation by Hazzard et al. (2002):

$$e_0 = \sqrt[3]{\frac{24k\pi \sum_{particles} R^2}{(1-n)\sum_{pipes} L}}, \tag{3}$$

where R is the particle radius, n is the mean porosity and L is the pipe (flow channel) length.

Fig. 7 Close-up view of numerical model showing circular particles of different size (average particle radius is 1 mm) and pore network model. Flow channels (solid segments at contacts between two particles) are connecting to neighbouring domains (pore spaces) bounded by a solid polygon. Black dots at the polygon centres are virtual pores where fluid pressure (P_f) is stored. The blue circles around those are proportional to magnitude of stored fluid pressure. The dotted polygon shows contributing segments used for calculating domain volume. Arrows are resultant forces applied to the particles surrounding the pore spaces due to fluid pressure P_f. Micro cracking due to fluid injection is represented as broken parallel bond contacts (dashed line) either in mode I or mode II. A chain of micro cracks builds up a visible macrocrack which can be bounded (area between two bold lines). For colour interpretation of this figure, the reader is referred to the web version of this paper

Fig. 8 Hydro-mechanical coupling in PFC^{2D} (m: particle mass; a: acceleration; k_c: contact stiffness, k_b: bond stiffness; U: particle overlap)

Fig. 9 Hydraulic aperture (e) versus normal stress (σ_n) of intact rock and foliation plane.

3.2. Model description

The coupling between hydraulically induced fracture propagation, fluid flow and foliation is studied through three rock mass models. The first model contains no foliation, i.e. the material is considered homogeneous and isotropic as well as serves as base model (case A in Fig. 10). In the second and third rock mass models (case B and C in

Fig. 10), smooth joint contacts are applied to simulate foliation. In model B smooth joints are parallel to S_H and in model C tilted by 15° clockwise with respect to S_H.

Field data presented in Section 2 suggest that the induced fracture propagated in the horizontal direction (parallel to sub-horizontal foliation) and therefore, 2D vertical sections of 2 m x 2 m are generated (Fig. 10). The chosen size of the rock model to the volume involved in *HF* stress measurement is an isolated, approx. one-meter-long open hole section. About 15.000 particles are generated in the models with the parameters listed in Table 2. Average particle size is about 1 mm, and, in agreement with grain size of typical mica schist from the Paks site.

The mechanical properties of the host rock is calibrated through a trial-and-error process described in Potyondy and Cundall (2004). The rock mass model without foliation is calibrated against laboratory data using the rock model described above (Table 3). According to Table 3, the calibrated Young's modulus, Poisson's ratio and Uniaxial Compressive Strength (*UCS*) are between measured minimum and maximum values, however, the Brazilian Tensile Strength (*BTS*) is somewhat higher in the rock mass model. This can be associated with the limited capability of PFC2D in complete matching of *UCS* to *BTS* ratio (Potyondy and Cundall 2004). On the other hand, the high variability in BTS is typical for foliated metamorphic rock, such as gneiss or mica schist (Zang and Berckhemer 1993).

Numerical microparameters in Table 2 are chosen to best resemble foliated mica schist and provide reasonable computation time as well. Foliations in this study are implemented as smooth-joints model which is a contact model that allows particles to slide past one another without over-riding one another (Mas Ivars et al. 2008). A joint is created by assigning this contact model to all contacts between particles that lie upon opposite sides of the joint surface. Length and number of joints are arbitrarily determined. The generated joint fabric is then overlaid on to the bonded particle assembly. Those particle contacts which were assigned with parallel bonds and located along the joint fabric are switched to smooth joint contacts and assigned with mechanical properties that are listed in Table 2. The length of each segment of joint set (0.2 m) is chosen arbitrarily in order to prevent model boundary effects. The rock mass model is pre-conditioned to have a bulk permeability of 10^{-18} m^2 that determines initial hydraulic aperture (e_0) in both rock matrix and foliation based on eq. (3).

Table 2 Parameters used in the bonded-particle numerical modelling with PFC [2D]

Table 3 Geomechanical laboratory data from ÁKMI et al. 2016 and simulation data

The chosen parameter value enables maintaining numerical stability, provides reasonable time steps and also, hydraulic aperture that shows good agreement with data derived from hydraulic field tests (Lemon et al. 2016). The pressure at both pore spaces (domains) connected by this broken contact is set to the average of those pressures. Therefore, it is assumed that the two pore spaces that were separated before the bond break become one space (Fig. 7).

Fig. 10 shows rock mass models A, B and C, in which the open hole interval between the packers is created by deleting particles in the center area with a size of 50 cm x 5 cm. Straddle packers are modelled as material regions above and below the open hole area by defining lower hydraulic aperture (1 nm, that is, impermeable) to prevent leak-off into the packers during injection. Furthermore, the particle contacts in the packer are treated stiffer and stronger than those contacts in the rock part to prevent fracturing (Table 2).

The applied in-situ stress field of the rock mass models agrees with the measured in-situ data (Section 2): the vertical stress ($S_v = S_{zz}$) equals 15 MPa and the maximum horizontal stress ($S_{Hmax} = S_{xx}$) equals 30 MPa.

Fig. 10 Three 2D numerical rock models with the in-situ stress field and idealized fluid front distributions. A: rock model without foliation; B: rock model with foliation parallel to orientation of maximum horizontal stress; C: rock model with foliation tilted by 15° with respect to maximum horizontal stress (S_{Hmax}). Injection point is in open test section created by deleting particles between upper and lower packers in the borehole. Injection fluid has a viscosity of 1 mPa s in rock model A (blue), and that of 10 mPa s in rock models B and C (cyan). For colour interpretation of this figure, the reader is referred to the web version of this paper

4. Simulation of injection procedure

Several injection cycles are performed to simulate injection phases and flow back. After injection, shut-in is simulated by stopping pumping and the interval pressure decreases as fluid leaks-off into stimulated rock mass. Since pressure relaxation always requires more time than to create or extend hydraulic fracture – especially for fluid with higher viscosity– the time for shut-in periods are set longer, i.e. double of that for injection in each model case. It must be noted that injected fluid cannot be removed from the borehole model, hence, interval

pressure will not decay to zero after any stimulation cycle. The simulation ends after the refracturing cycle as the induced hydraulic fracture reaches model boundary.

Hydraulic fracturing of a given interval in a borehole is modelled as fluid being injected into an unpressurized hydraulic domain (Section 3.1). This is located at the center of the open borehole section as well as the rock mass model, which is represented by particles deleted between the sealing packers. Injected fluid may flow from the stimulated central domain to those which are directly connected.

Figure 10 illustrates how water - with viscosity of η = 1 mPa s - is injected into model A, in rock mass without foliation. In model B and model C, drilling mud with viscosity of η =10 mPa s, is used for stimulation into rock mass with pre-existing foliation. In all models the injection flow rate is set to 3.6 l/min according to the applied flow rate of the field tests (Table 4).

Hydro-mechanical processes during simulation of injection are studied through spatial-temporal monitoring of fluid pressure evolution and micro crack generation process. Micro crack generation due to failure at either parallel or smooth joint contacts are observed simultaneously. The chain of micro cracks are identified visually as a macrocrack. Micro cracks induced due to fluid injection may be origin of pure tension (Mode I) or shearing (Mode II) at either contact type.

5. Modelling results

Results of numerical simulation of *HF* into crystalline rock mass are presented as flow rate (Q), injected fluid volume (V_{inj}), interpreted pressures, like fracture breakdown pressure (*FBP*) and refracturing pressure (*RFP*), type and amount of generated micro cracks as well as field testing data are summarized in Table 4. The results are detailed for each rock mass model, i.e. homogeneous rock mass (A), rock mass with horizontal foliation (B) and sub-horizontal (C) foliation.

For each model, general observations based on monitored interval pressure and time-dependent number of generated micro cracks for the pressurization cycles are presented first. This is followed by analyzing the spatial distribution of micro and macro cracks for each of the models.

Table 4 Summary of simulation models and field data as well as generated type and ratio of micro cracks at the end of hydraulic fracturing. Q: injection flow rate, V_{inj}: total injected volume, *FBP*: fracture breakdown pressure, *RFP*: refracturing or fracture reopening pressure

5.1. Stimulation of homogeneous rock mass model A by water injection

Interval pressure, flow rate and cumulative number of generated micro crack records of model A are presented in Fig. 11. The results show that minor fracturing occurs during the first injection cycle. This is reflected by relatively low increase in number of induced micro cracks versus time associated with two distinct pressure drops in the order of 1 to 2 MPa. Although pressure drops are observed during this stimulation cycle, no characteristic pressure signature of fracture breakdown and subsequent fracture propagation is visible in the pressure versus time record. Therefore, the first cycle is interpreted as a cycle in which tensile fracture initiates. After shut-in, micro crack generation stops.

The second injection cycle shows a clear pressure drop and subsequent pressure undulation (Fig. 11) during continuous flow. This is interpreted as fracture breakdown pressure (*FBP*) at a peak pressure of 24 MPa which is followed by fracture propagation until injection is stopped at 21.5 MPa. After this injection phase, minor micro crack generation can be seen in Fig. 11, in contrast to the shut-in phase of cycle 1.

The last injection cycle exhibits a peak pressure of 21.5 MPa and short pressure undulation at about 21 MPa, (Fig. 11). The refracturing pressure (*RFP*), therefore, is considered to be 21.5 MPa which is lower than the *FBP* and similar to the fracture initiation pressure of the first cycle. The duration of the last cycle is shorter as the induced hydraulic fracture reaches model boundary. Few cracks are generated during reopening and no cracks are observed during shut-in.

Figure 12 provides information about the generation of microfractures during pressurization of model A with water at two stages, fracture breakdown (A/1) and refracturing (A/2). Stage A/1 in Fig. 12 demonstrates that several micro cracks are induced in tension close to the boundary region between the sealing packers, open borehole area and the rock mass. Furthermore, a chain of microscopic tensile micro cracks on the right side of the model region builds a macroscopic hydraulic fracture. This is extended during the fracturing and refracturing cycles, approx. parallel to the direction of maximum principal stress, the maximum horizontal stress (S_{Hmax}). The undulation in the hydraulic fracture propagation reflects inherent variability in strength of the particles and parallel bond contacts representing the rock mass.

Fig. 11 Interval pressure, flow rate and cumulative number of micro cracks versus time (dashed) of PFC ^{2D} simulation in model A (simulation of homogeneous rock mass by water injection) with identified fracture breakdown pressure *FBP* and reopening pressure *RFP*. Vertical lines show onset of injection and shut-in phases. Stages A/1 and A/2 show the occurrence of fracture breakdown and refracturing, respectively.

Fig. 12 Snapshots of micro cracking process in model A (homogeneous rock mass) at time stages A/1 (fracture breakdown) and A/2 (refracturing) of the pressure versus time recording presented in Fig.11. Stage A/1 shows micro cracks induced close to the packers (indicated by black circles) as well as initiation and propagation of hydraulic fracture at time stage. At stage A/2, the induced hydraulic fracture reaches model boundary. All particles except for those representing straddle packers above and below the open borehole interval (black) are removed for enhanced visibility. The vertical stress (S_v) equals 15 MPa and the maximum horizontal stress (S_{Hmax}) equals 30 MPa. Micro crack symbols, red: parallel bond normal failure, cyan and magenta: smooth joint normal and shear failure, respectively. Foliation planes (smooth joint contacts) are shown in grey. For color interpretation of this figure, the reader is referred to the web version of this paper

5.2. Mud injection into model B with horizontal foliation

The interval pressure, flow rate and generated micro crack records for simulation of model B are presented in Fig. 13. In this model horizontal foliation is parallel to direction of maximum horizontal stress and the rock mass is pressurized by drilling mud with a viscosity of 10 mPa s.

The first injection cycle in Fig. 13 exhibits a first breakdown peak pressure *FBP* of 17 MPa, which is followed by a pressure reduction to 13.5 MPa. Shortly after this pressure drop, the flow is shut-in. Micro crack generation begins before reaching peak pressure and after shut-in the number of micro cracks increases steadily. Based on these observations, the first injection cycle can be interpreted as breakdown cycle with a *FBP* of 17 MPa.

The pressure versus time record of second stimulation cycle in Fig. 13 exhibits a refracturing pressure *RFP* of 19 MPa. Small pressure drop before reaching *RFP* can be observed as well. Undulating pressure of approximately 17-18 MPa following *RFP* indicates hydraulic fracture propagation that can be caused by differences in strength and permeability of the foliation planes in the rock mass. Therefore, this cycle is interpreted as refracturing cycle with a *RFP* of 19 MPa, which is higher than the *FBP*. After shut-in of the refracturing cycle, only relatively small amount of micro cracks are generated.

Figure 14 gives insight into the generation of microfractures during pressurization of model B with mud at two stages, fracture breakdown (B/1) and refracturing (B/2). After the first, breakdown cycle, induced micro cracks are observed around the boundary of sealing packers, open borehole area and rock mass, as well as partly at the horizontal foliation planes (stage B/1 in Fig. 14). The cracks are mostly induced in tension. An initiation of a newly induced hydraulic fracture is visible around the open borehole area between two foliation planes. After shut-in in refracturing cycle (stage B/2 in Fig. 14), fractures are extended both in the rock mass and foliation planes, parallel to the maximum principal stress S_{Hmax}. The tensile hydraulic fracture in the rock mass propagates to a greater extent. The foliation planes are fractured mostly in tension, a fracturing mechanism which is expected for hydraulic fracturing. Shear micro cracks are also generated, however, their relative smaller portion to tensile micro cracks may suggest that the foliation planes are not optimally oriented for hydro-shearing.

Comparison of interval pressures during cycle 1 and 2 (Fig. 13) with micro crack distribution (Fig. 14) shows that as soon as the mud penetrates the foliation planes, the interval pressure remains high. This implies that higher fluid pressure is required to pump the mud into the foliation and to the rock mass. This explains the higher *RFP* compared to the *FBP* of this stimulation with high viscous mud.

Fig. 13 Interval pressure, flow rate and cumulative number of generated micro cracks versus time (dashed) for simulation of model B (injection of drilling mud in to rock mass with horizontal foliation) with identified fracture breakdown pressure, *FBP* (B/1) from the first cycle and slightly larger reopening or refracturing pressure R*FP* (B/2*)* from the second cycle. Vertical lines show onset of injection and shut-in phases.

Fig. 14 Snapshots of micro cracking process in simulation case B (stimulation of rock mass with horizontal foliation by drilling mud) at 2 points in time, occurrence of fracture breakdown and reopening, near borehole area (stages B/1 and B/2 in Fig. 13). Stage B/1 shows micro cracks induced close to the packers (indicated by black circles), stimulated foliation (indicated by black rectangles) as well as induced hydraulic fracture. Stage B/2 illustrates propagation of hydraulic fracture. All particles except for those representing straddle packers above and below the open borehole interval (black) are removed for enhanced visibility. The vertical stress (S_v) equals 15 MPa and the maximum horizontal stress (S_{Hmax}) equals 30 MPa. Micro crack symbols, red: parallel bond normal failure, cyan and magenta: smooth joint normal and shear failure, respectively. Foliation planes (smooth joint contacts) are shown in grey. For color interpretation of this figure, the reader is referred to the web version of this paper

5.3. Mud injection into model C with slightly inclined foliation

The interval pressure, flow rate and generated micro crack (dashed) records for model C are summarized in Fig. 15. In this simulation case the rock mass contains foliation tilted by 15° with respect to direction of maximum horizontal stress. Drilling mud is represented as a fluid with viscosity of 10 mPa s.

Figure 15 shows the pressure increase during injection until shut-in and relatively slow pressure decay after that of the first injection cycle. The evolution of number of generated micro cracks suggests minor fracturing during injection starting at a pressure level of approx. 15 MPa. The crack generation process continues at a faster rate throughout the shut-in period of the first cycle. Consequently, the first cycle is interpreted as a phase in which tensile fracture initiates at a fracture initiation pressure (*FIP*) of 15 MPa that equals the minimum stress in the model which corresponds to the vertical stress, S_v in the field.

The second injection cycle initially shows a few minor pressure drops that are followed by breakdown *FBP* (C/1) at 30 MPa and characteristic pressure drop to 23 MPa at shut-in (Fig. 15). The peak pressure is interpreted as the *FBP* which is followed by fracture propagation until injection is stopped. Therefore, this injection cycle can be considered as breakdown cycle. After the injection phase, micro crack generation continues during shut-in.

The third injection cycle shows a peak pressure at 27 MPa which is interpreted as the *RFP* (C/2) which is slightly lower than the *FBP* (C/1). Interestingly, more micro fractures are generated during the shut-in period than during injection. This can be an artefact due to fracturing close to the model boundary.

Figure 16 provides information about the generation of micro cracks during pressurization of model C with mud at two stages, fracture breakdown (C/1) and refracturing (C/2). Micro cracks at stage C/1 are induced around the boundary between the sealing packers, open borehole area and rock mass, as well as at the sub-horizontal foliation planes. Hence, an initiation of a newly induced, tensile hydraulic fracture in the rock mass and stimulated foliations are visible at fracture breakdown stage in Fig. 16. The micro crack evolution during breakdown and refracturing cycles (stages C/1and C/2 in Fig. 16) indicate that fractures are extended both in the rock mass and foliation planes, approximately parallel to the maximum principal stress S_{Hmax}. The tensile hydraulic fracture in the rock mass propagates to a greater extent. The foliation planes are fractured in tension as the main stimulation mechanism. Shear fracturing, therefore, is not the main fracturing mechanism, since the planes of weakness are not optimally oriented for hydro-shearing.

Comparing Fig. 15 to Fig. 16, the evolution of fluid pressure suggests that as the mud penetrates the foliation planes, the fluid pressure remains high. Higher fluid pressure is required to pump the mud into the foliation and, therefore, to reopen and extend the tensile hydraulic fracture at the tip of the foliation. Although pressure build up is partitioned between the domains located at the smooth joint and parallel bond contacts, it requires less hydraulic energy to extend the initial tensile hydraulic fracture throughout the parallel bond contacts representing the rock mass. This explains the high *FBP* and *RFP* as well as the lower *RFP* compared to *FBP* of this stimulation with high viscous mud.

Fig. 15 Interval pressure, flow rate and cumulative number of generated micro cracks versus time (dashed) records for simulation of model C (mud injection of rock mass with slightly inclined foliation by) with identified fracture breakdown pressure, *FBP(C/1)* and reopening or refracturing pressure *RFP(C/2).* Vertical lines show onset of injection and shut-in phases.

Fig. 16 Snapshots of micro cracking process in simulation case C (stimulation of rock mass with sub-horizontal foliation by drilling mud) at 2 points in time, occurrence of fracture breakdown and reopening, near borehole area (stages C/1 and C/2 in Fig. 15). Stage C/1 shows micro cracks induced close to the packers (indicated by black circle), stimulated foliation (indicated by black rectangles) as well as induced hydraulic fracture. Stage C/2 illustrates propagation of hydraulic fracture. All particles except for those representing straddle packers above and below the open borehole interval (black) are removed for enhanced visibility. The vertical stress (S_v) equals 15 MPa and the maximum horizontal stress (S_{Hmax}) equals 30 MPa. Micro crack symbols, red: parallel bond normal failure, cyan and magenta: smooth joint normal and shear failure, respectively. Foliation planes (smooth joint contacts) are shown in grey. For color interpretation of this figure, the reader is referred to the web version of this paper

6. Discussion

6.1. Comparison of simulation results for the three models

Table 4 shows that the injected volume of fluids during numerical simulation of hydraulic fracturing (*HF*) in models with foliation (model B and C) is about one order of magnitude smaller than that on field testing. In case A (simulation of homogeneous rock mass by water injection) the pressure versus time record agrees with injected rate and volume recorded on field testing. The lower injected fluid volume in the rock models with foliation is the result of using 2D section for the interval in the borehole, i.e. the lack of fluid flow in the out-of-plane direction. Consequently, this is a clear limitation of the 2D version of the numerical code and should be subject of future

development. We should note that field data include recorded flow back rate (Fig. 5b), however, this is not simulated in present study. This is not required, since these data cannot be used for the numerical study as the flow back was interrupted to check the sealing condition of the packers. Hence, matching flow rate records from field tests and numerical simulation with the 2D version of codes is not relevant.

The peak pressures, i.e. measured fracture breakdown (*FBP*) and refracturing pressure (*RFP*) are different for each simulation case. In case A with homogeneous rock mass the *FBP* is higher than the *RFP*, i.e. the model shows good agreement with the classical pressure-time record of hydraulic fracturing (Fig. 11). On the other hand *FBP* and *RFP* are somewhat higher than those observed in field testing which implies that pre-existing fractures in the numerical rock mass models are required to reproduce these pressure values. This is supported by model case B for which the simulated *FBP* and *RFP* agree with field data (Table 4). Not only the magnitudes show good match, but also the numerical code is able to capture the higher *RFP* for a rock mass with horizontal foliation.

Interestingly, when simulating model case C with tilted plane of foliation, the *RFP* is lower than the *FBP*; and both values are higher than that recorded pressure from field testing (Table 4). The higher *FBP* can be explained in a way that the area of tilted foliation planes to be fractured is higher compared to the case in which the foliation planes are horizontal, consequently the tilted foliation has larger volume for fluid storage. The higher *FBP* with higher fracture inclination angle agrees with the modelling results presented by Lavrov et al. (2016). On the other hand, this might also be related to the limitation of the 2D version of the numerical code. Therefore, further investigations are required.

The peak pressure during the first injection cycle in homogeneous model A and in in model C with tilted foliation is not interpreted as *FBP* although a pressure drop of several MPa is observed, see Fig. 11 and Fig. 15. This is the case for which the fracture initiation around the borehole is affected by the strength contrast between the rock mass and the packers. Due to the pressure drop, the injection must be stopped to avoid numerical instability. This limitation is overcome by pressure relaxation after shut-in which is followed by injection at the same flow rate.

The results presented in Table 4 and Fig. 12 show that only parallel bonds break in simulation of model A, which is expected for hydraulic fracturing of homogeneous rock mass. The portion of different failure types at parallel bonds and smooth joints for model case B and C suggest (Fig. 14 and Fig. 16) that the fracturing processes are different in these models. Although the dominant type of fracturing is tensional for a rock mass with foliation, shear micro cracks are also generated. The lower number of shear fractures suggest that the foliation planes are

not optimally oriented for hydro-shearing. Our numerical modelling results show that fracture initiation develop from the stiffness and strength contrast between packers in the borehole and the surrounding rock mass. Furthermore, the low tensile strength of foliation planes in the rock mass may contribute to this. Consequently, our results confirm the results and interpretations of field tests described by Healy and Zoback (1988) and Hickman and Zoback (1983). Similar to our findings, they linked the anomalous breakdown pressure to lower tensile strength and anisotropy of the rock mass.

6.2. Hypothesis of viscous blocking

The results of coupled numerical modelling show that orientation of rock foliation with respect to direction of major principal stress affects hydraulic fracturing results. The fracture breakdown pressure and refracturing pressure seem to be inversely proportional to angle between foliation and maximum in-situ stress which agrees with the observation made by Lavrov et al. (2016).

Considering the results of all simulated models (A, B and C), and the discussion above, the rock mass with horizontal foliation (model B) injected by high viscosity mud shows best fit with field data. The atypical field observation with higher RFP in the second cycle of pressurization can be explained by the injection of high viscous fluid (mud) and existing foliation in the mica schist. First, injected mud flows into foliation plane, remains there and blocks the flow. Mud flows into the initial tensile fracture induced within a weaker area in the rock mass close to the packer and interval and propagates the initiated fracture during the fracturing cycle. Due to the presence of mud in the foliation planes, higher RFP is required to reopen the tight foliation planes and to create and to extend fractures in subsequent refracturing cycles. However, when the foliation is inclined (model C), the shearing does not provide large hydraulic aperture increase to let the viscous mud in, compared to the horizontal foliation. This may explain why simulation of injection into tilted foliation with high viscous mud does not explain the atypical field data.

7. Conclusions

In this study, an atypical behavior of hydraulic fracturing tests in low permeable mica schist is investigated. The field data from site investigations in Hungary show that the fracture breakdown pressure (*FBP*) is lower than the refracturing pressure (*RFP*) of the subsequent injection cycles for one and the same flow rate. This field observation motivated the application of the Particle Flow Code (PFC^{2D}) to study the atypical hydraulic fracturing behavior in a series of two-dimensional models subjected to several injection cycles. The effect of foliation and its

orientation with respect to the direction of maximum horizontal stress and the viscosity of injected fluid (drilling mud) on breakdown and refracturing pressures is tested through different rock mass models.

The modelling results show that homogeneous rock mass that is stimulated by water pressure follows the classical principle of hydraulic fracturing with an induced hydraulic fracture that propagates parallel to the direction of maximum principal stress. However, the results of the models that are foliated parallel to maximum principal stress and stimulated by mud suggest that foliation and high viscosity fluid are required to match the field observations. We argue that the drilling mud penetrates the sub-horizontal foliation plane and makes the opened fracture tight by an effect which is referred to as viscous blocking. The process prevents leak-off from the opened hydrofracture that can explain the increased *RFP* in subsequent cycles. On the other hand when the rock mass has dipped foliation and is stimulated by mud, the RFP is lower than the FBP. This might be explained by hydroshearing with foliation that is not optimally oriented compared to the horizontal foliation.

The study shows that crack development and progression in cases where foliation is present reflects that in-situ stress measurements require further understanding. Therefore, sensitivity of orientation, length and strength (stiffness) of foliation as well as stress regime configuration, flow rate, fluid density and well orientation must be also tested in a future study. This may contribute to a more precise stress determination and analysis method.

Acknowledgements

The work was kindly supported by Golder Associates Hungary.

References

ÁKMI Ltd (2016) Conduction of Geological Research Program Required for Paks II Site Permit. Final report of the Geological Research Program. Document ID: MÁ/PA2-16-FT-14 V2 (Paks II Telephelyengedélyének Megszerzéséhez Szükséges Földtani Kutatás Végrehajtása. Földtani Kutatási Program Zárójelentése, in Hungarian), Pécs, Hungary

Amadei B, Stephansson O (1997) Rock stress and its measurement, Chapman & Hall, London

Doe TW, Korbin GE (1987) A Comparison of Hydraulic Fracturing and Hydraulic Jacking Stress Measurements, 28th US Symp on Rock Mech, Tuscon, 283–290

Haimson BC, Cornet FH (2003) ISRM Suggested Methods for rock stress estimation – Part 3: Hydraulic Fracturing (HF) and/or hydraulic testing of pre-existing fractures (HTPF), International Journal of Rock Mechanics and Mining Sciences, 40:1011-1020

Hazzard JF, Young RP, Oates SJ (2002) Numerical modeling of seismicity induced by fluid injection in a fractured reservoir, In Proceedings of the 5th North American Rock Mechanics Symposium Mining and Tunnel Innovation and Opportunity, Toronto, ON, Canada, 7–10 July 2002, 1023–1030

Healy JH, Zoback MD (1988) Hydraulic fracturing in–situ stress measurements to 2.1 km depth at Cajon Pass, California, Geophys Res Let, 15:1005–1008

Hickman SH, Zoback MD (1983) The interpretation of hydraulic fracturing pressure-time data for in-situ stress determination, in Hydraulic Fracturing Measurements (ed. by Zoback MD, Haimson BC), National Academy Press, Washington D.C., 44–54

Hökmark H, Lönnqvist M, Fälth B (2010) THM–issues in repository rock. Thermal, mechanical, thermo–mechanical and hydro–mechanical evolution of the rock at the Forsmark and Laxemar sites. Technical Report, TR–10–23, SKB Publications, 2010, Updated 2011-10

Itasca Consulting Group Inc (2008) PFC2D version 4.0 Manual (Particle Flow Code in 2 dimensions), Minneapolis, USA

Itasca Consulting Group Inc (2012) Technical Memorandum to PFC2D (Particle Flow Code in 2 dimensions) version 4.0 – 5.0 Parallel Bond Enhancement, Minneapolis, USA

Labuz J, Zang A (2012) ISRM suggested methods for rock failure. Mohr–Coulomb failure criteria, Rock Mech Rock Eng, 45:975–979

Lavrov A, Larsen I, Bauer A (2016) Numerical modelling of extended leak–off test with a pre-existing fracture, Rock Mech Rock Eng, 49:1359–1368

Lemon M, Farkas MP, Korpai F, Dankó G (2016) Technical report of hydraulic fracturing tests. Conduction of Geological Research Program Required for Paks II Site Permit, Golder Associates Hungary, Budapest, Hungary

Lin C, He J, Li X,, Wan X, Zheng B (2017) An experimental investigation into the effects of the anisotropy of shale on hydraulic fracture propagation, Rock Mech Rock Eng, 50:543–554

Mas Ivars D, Potyondy DO, Pierce M, Cundall, PA (2008) The smooth–joint contact model. Proceedings of the 8th World Congress on Computational Mechanics – 5th European Congress on Computation Mechanics and Applied Science and Engineering, Venice, Italy, 2008

Potyondy DO, Cundall PA (2004) A bonded–particle model for rock, Int J Rock Mech Min Sci, 41:1329–1364

Shimizu H, Murata S, Ishida T (2011) The distinct element analysis for hydraulic fracturing in hard rock considering fluid viscosity and particle size distribution, Int J Rock Mech Min Sci, 48:712–727

Stephansson O, Zang A (2012) ISRM suggested methods for rock stress estimation – Part 5: Establishing a model for the in-situ stress at a given site. Rock Mechanics and Rock Engineering 45, 955-969

Yoon JS, Zang A, Stephansson O (2014) Numerical investigation on optimized stimulation of intact and naturally fractured deep geothermal reservoirs using hydro–mechanical coupled discrete particles joints model, Geothermics 52:165–184

Yoon JS, Zang A, Stephansson O, Hofmann H, Zimmermann G (2017) Discrete element modelling of hydraulic fracture propagation and dynamic interaction with natural fractures in hard rock, Procedia Engineering, 191: 1023–1031

Zang A, Berckhemer H (1993) Classification of crystalline drill cores from the KTB deep well based on strain, velocity and fracture experiments, Int J Rock Mech Min Sci, 30(4): 331–342

Zang A, Stephansson O (2010) Stress field of the Earth's crust. Dordrecht, Springer

Zang A, Stephansson O, Heidbach O, Janouschkowetz S (2012) World stress map data base as a resource for rock mechanics and rock engineering, Geotechnical and Geological Engineering, 30(3): 625–646.

Zhou J., Zhang L, Braun A, Han Z (2016) Numerical modeling and investigation of fluid-driven fracture propagation in reservoirs based on a modified fluid-mechanically coupled model in two-dimensional Particle Flow Code, Energies, 9(9), 699

Zhou L, Ding L, Guo Q (2016) Indoor experiments on the effect of the slurry on the in–situ stress measurement results, in: Johansson E, Raasakka V (Eds.), Symposium Proceedings, 7th International Symposium on In–Situ Stress, Tampere, Finland, May 10–12, 2016, 235–246

Zoback MD (2010) Reservoir Geomechanics. Cambridge, Cambridge University Press

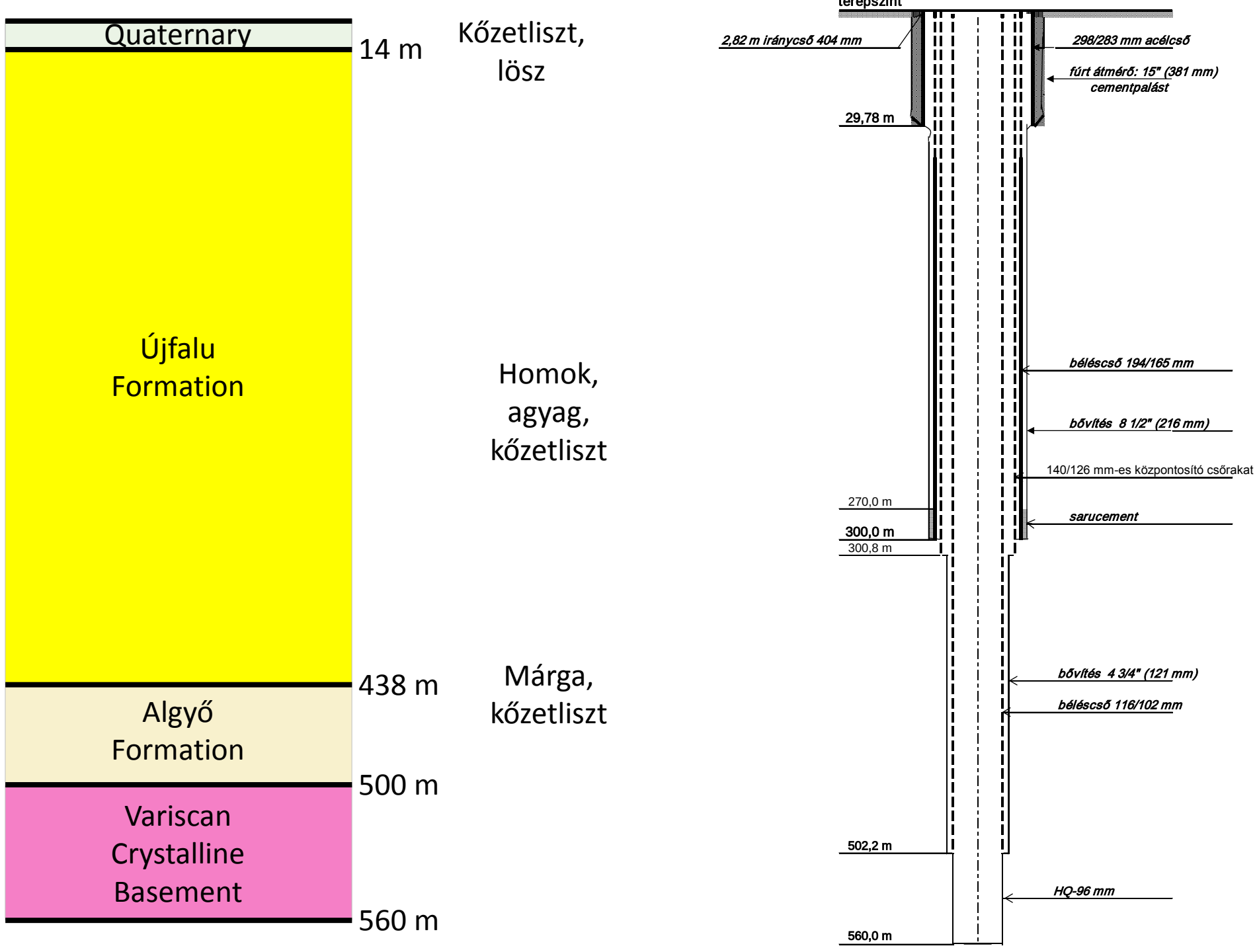
Quaternary
14 m
Kőzetliszt, lösz
Újfalu Formation
Homok, agyag, kőzetliszt
438 m
Algyő Formation
Márga, kőzetliszt
500 m
Variscan Crystalline Basement
560 m
terepszint
2,82 m iránycső 404 mm
298/283 mm acélcső
fúrt átmérő: 15" (381 mm)
cementpalást
29,78 m
béléscső 194/165 mm
bővítés 8 1/2" (216 mm)
140/126 mm-es központosító csőrakat
270,0 m
sarucement
300,0 m
300,8 m
bővítés 4 3/4" (121 mm)
béléscső 116/102 mm
502,2 m
HQ-96 mm
560,0 m

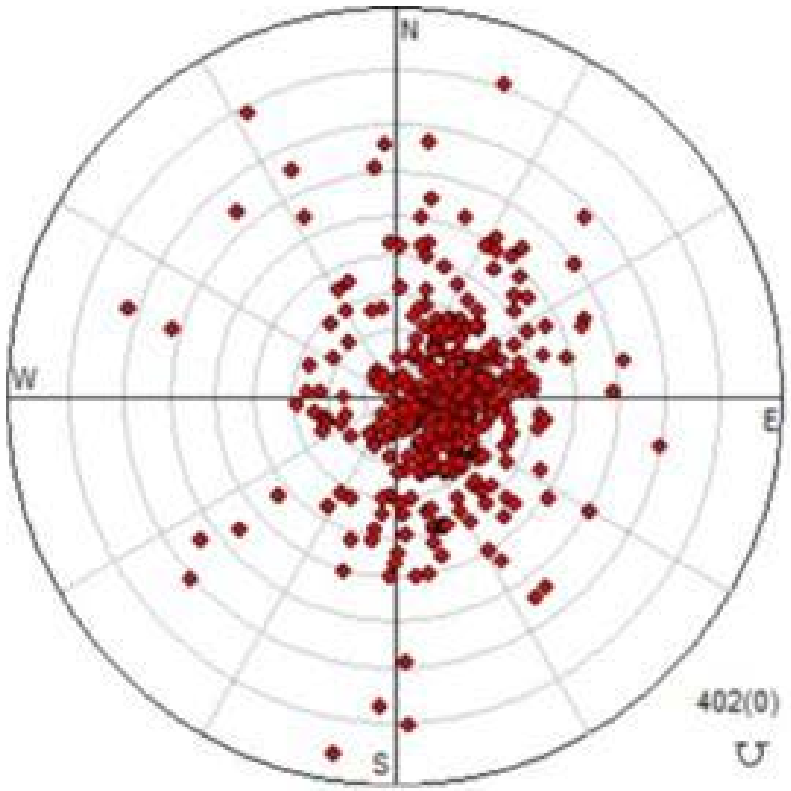
N
W
E
S
402(0)

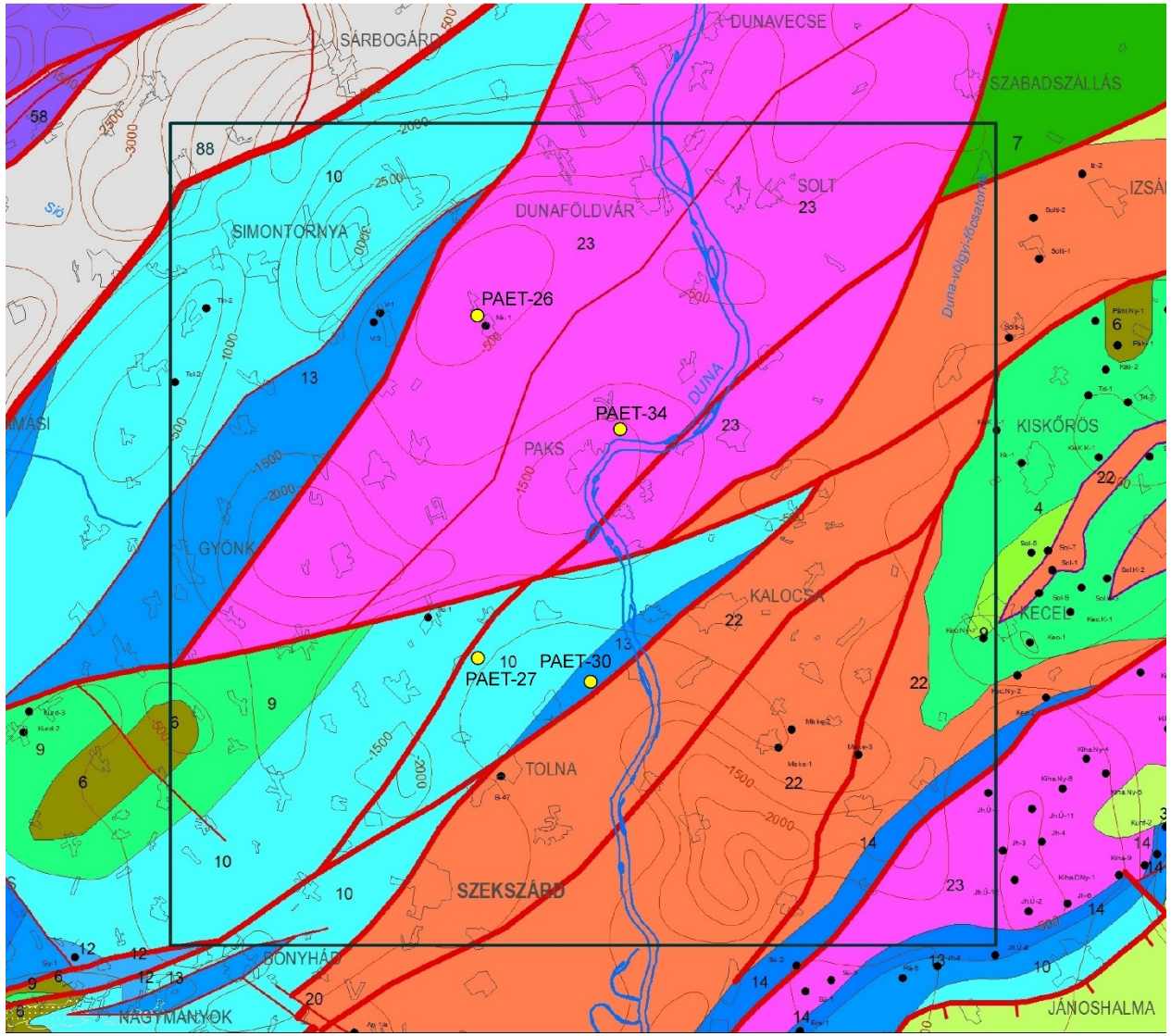
DUNAVECSE
SÁRBOGÁRD
SZABADSZÁLLÁS
SIMONTORNYA
DUNAFÖLDVÁR
SOLT
PAET-26
PAET-34
PAKS
DUNA
Duna-völgyi-főcsatorna
KISKŐRÖS
KALOCSA
KECEL
PAET-27
PAET-30
TOLNA
SZEKSZÁRD
BONYHÁD
NAGYMANYOK
JÁNOSHALMA
GYÖNK
Sió

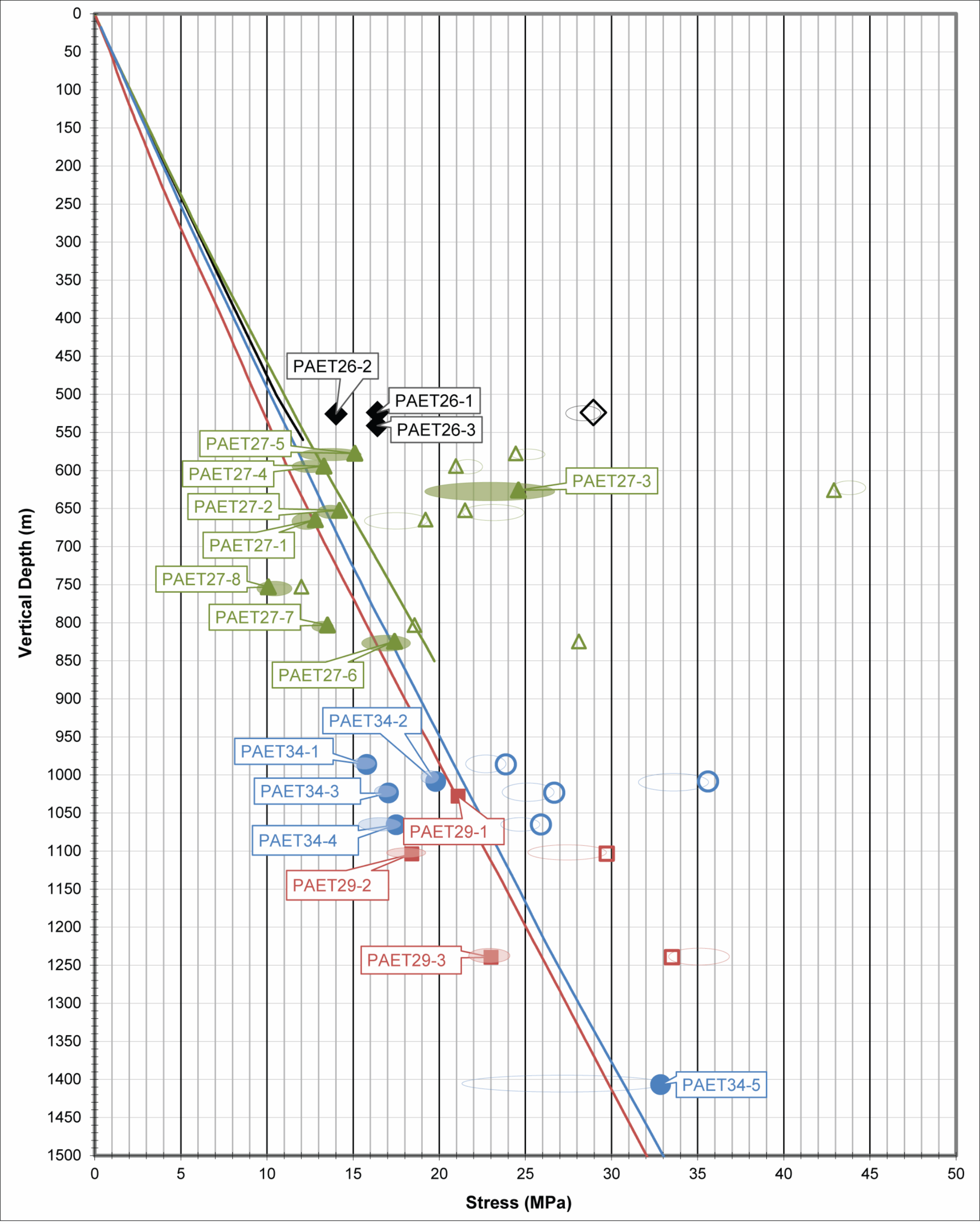

PAET-26 Minimum and Maximum Horizontal Stress

PAET-27 Minimum and Maximum Horizontal Stress

PAET-29 Minimum and Maximum Horizontal Stress

PAET-34 Minimum and Maximum Horizontal Stress

Range of Calculated Stress

Lithostatic Gradient by Borehole

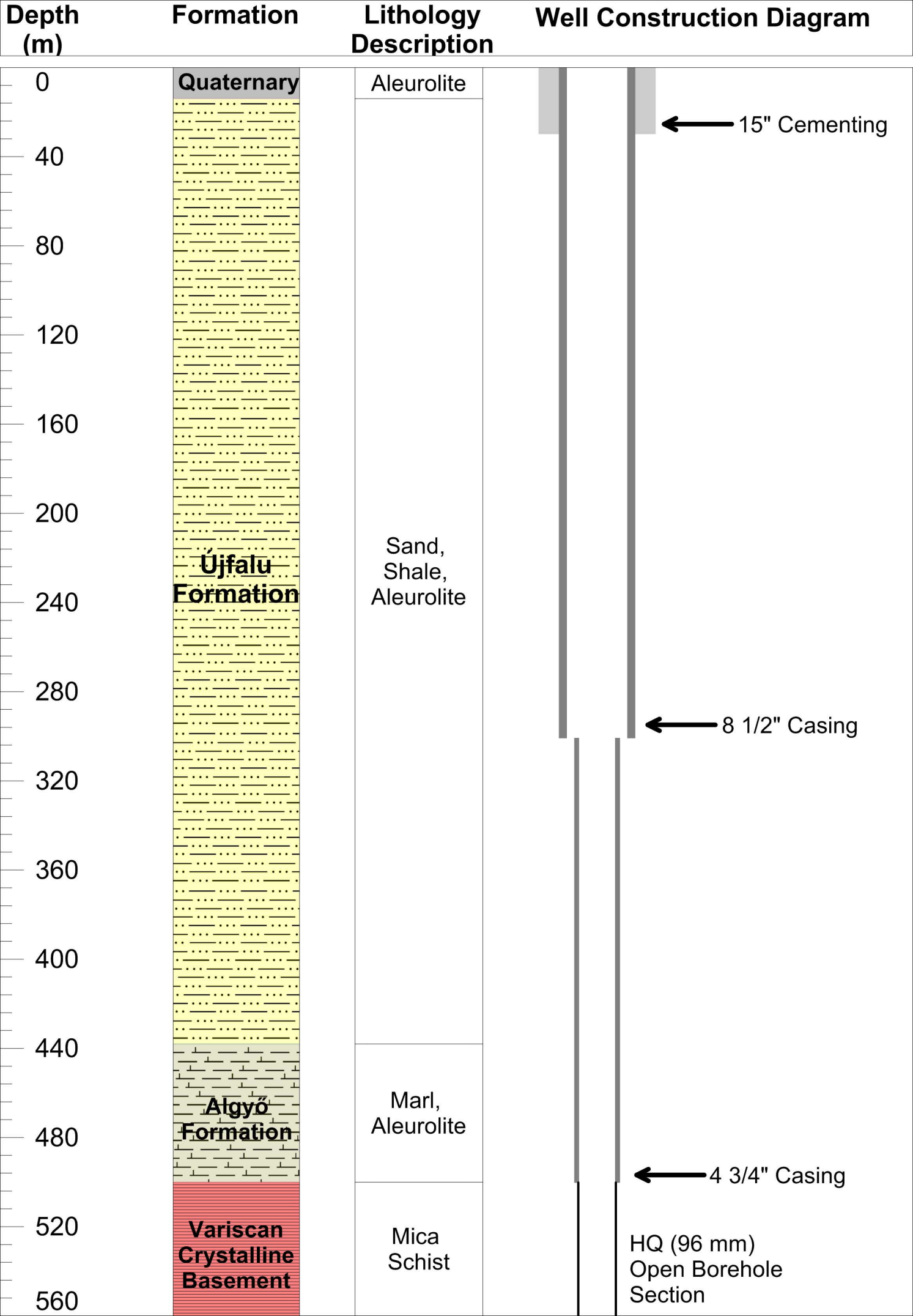
Depth (m)
Formation
Lithology Description
Well Construction Diagram
0
40
80
120
160
200
240
280
320
360
400
440
480
520
560
Quaternary
Újfalu Formation
Algyő Formation
Variscan Crystalline Basement
Aleurolite
Sand, Shale, Aleurolite
Marl, Aleurolite
Mica Schist
15" Cementing
8 1/2" Casing
4 3/4" Casing
HQ (96 mm) Open Borehole Section

Depth (m)

Pre-testing BHTV Image Logs

Traveltime Log

0° 90° 180° 270° 0°

Amplitude Log

0° 90° 180° 270° 0°

Position

Post-testing BHTV Image Logs

Amplitude Log

0° 90° 180° 270° 0°

Traveltime Log

0° 90° 180° 270° 0°

539.2

539.6

540.0

540.4

540.8

541.2

541.6

542.0

542.4

542.8

a

FIT Frac Refrac1 Refrac2 Invalid Refrac3 Jacking Refrac4

1 2 3 4 5 6

Interval pressure (MPa)

Flow rate (l/min)

0 5 10 15 20 25

0 4 8 12 16 20

0 60 120 180 240 300 360

Flow time (min)

Fig. 5b

b

Cycle 1: Breakdown

Cycle 2: Refracturing

Injection

Shut-in

Flow back

FBP

RFP

SIP

Interval pressure (MPa)

Flow rate (l/min)

Flow time (min)

0

5

10

15

20

0

3

6

9

12

15

35

40

45

50

55

60

65

70

75

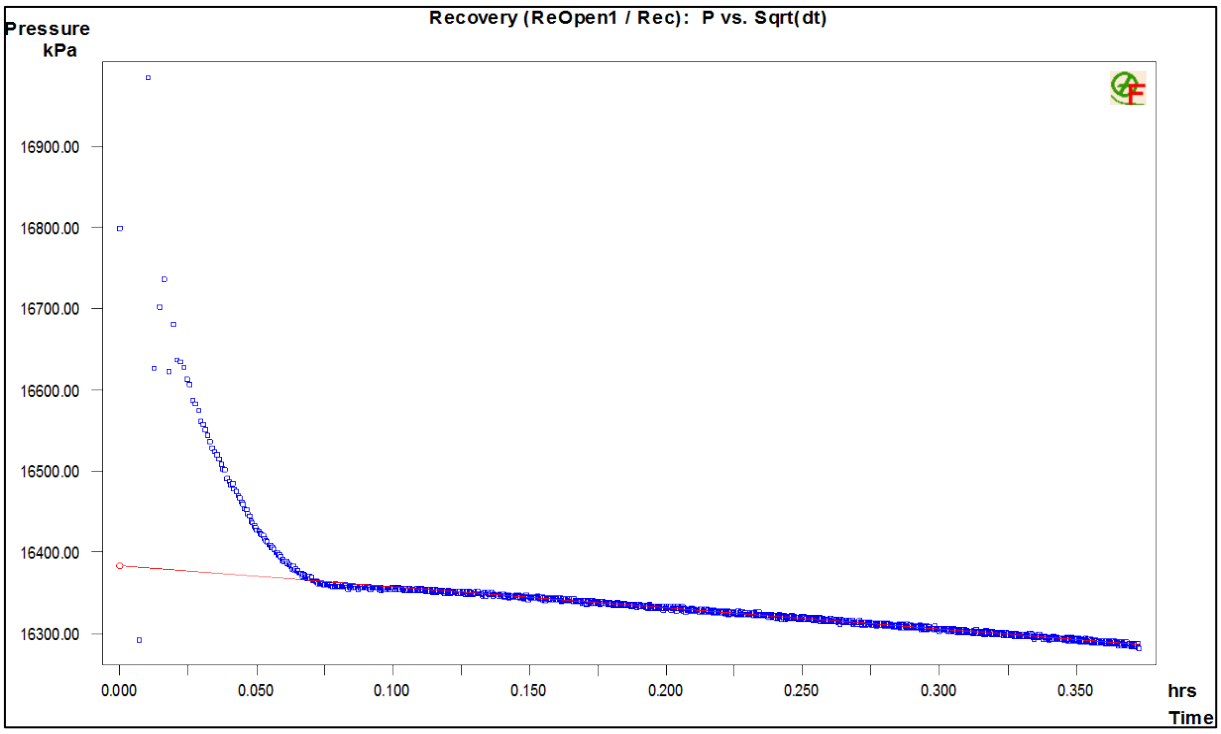

Figure 6a

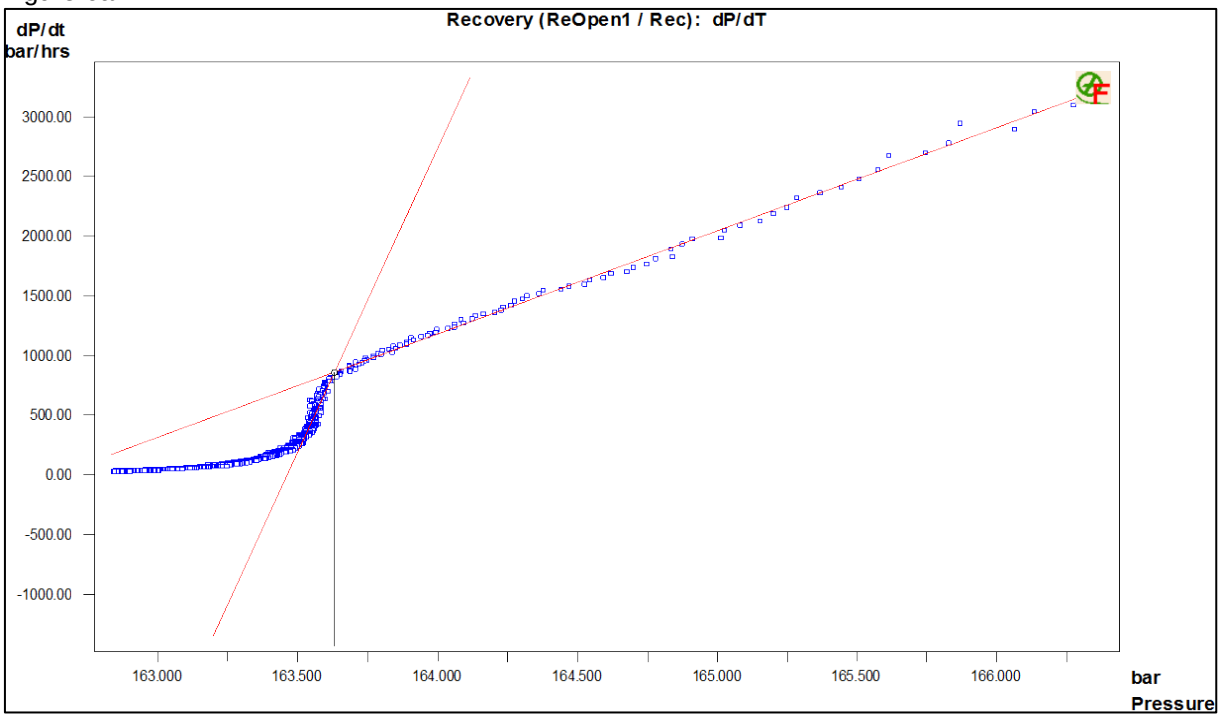

Figure 6b

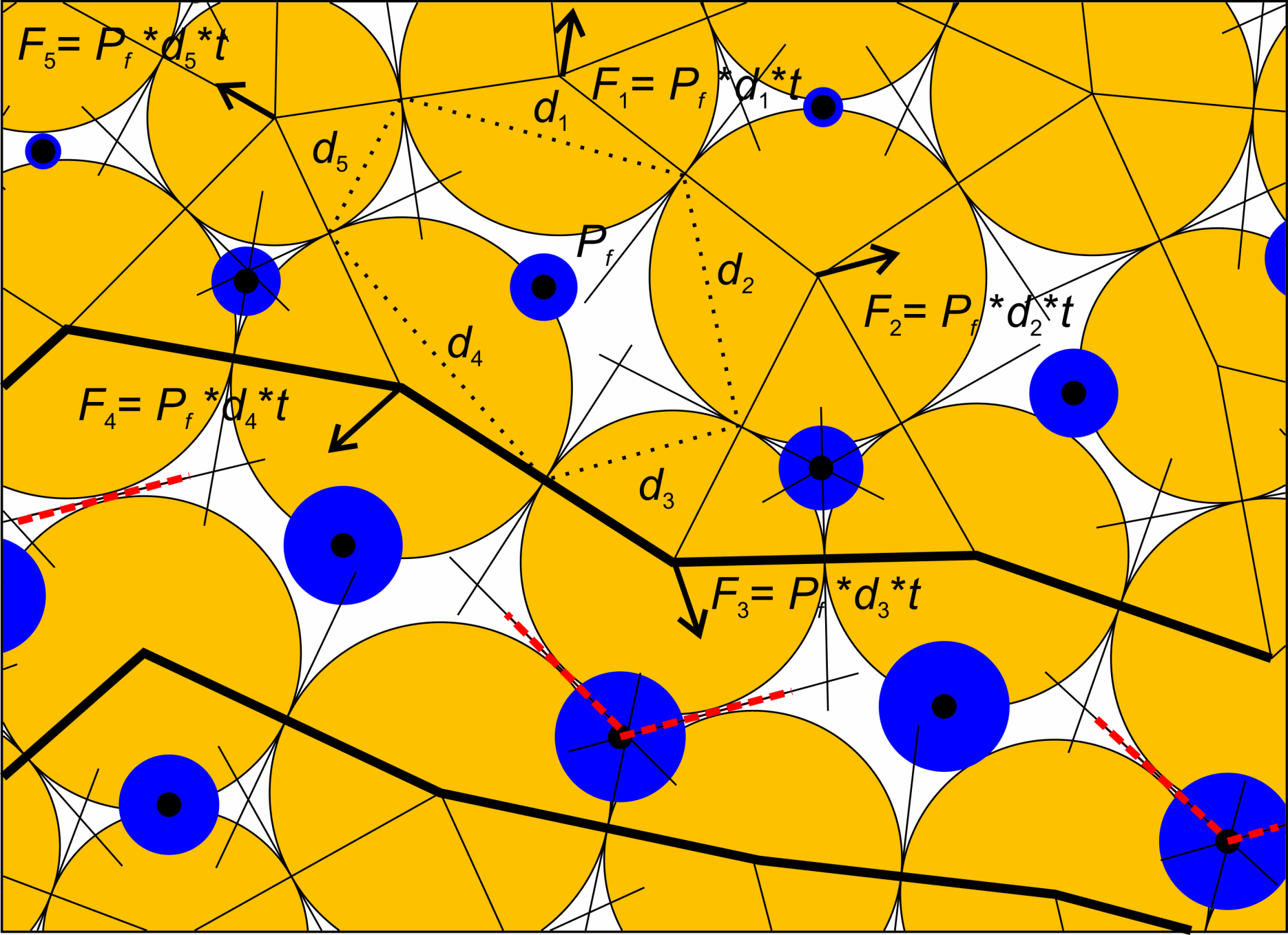
$F_5 = P_f * d_5 * t$
$F_1 = P_f * d_1 * t$
d_1
d_5
P_f
d_2
$F_2 = P_f * d_2 * t$
d_4
$F_4 = P_f * d_4 * t$
d_3
$F_3 = P_f * d_3 * t$

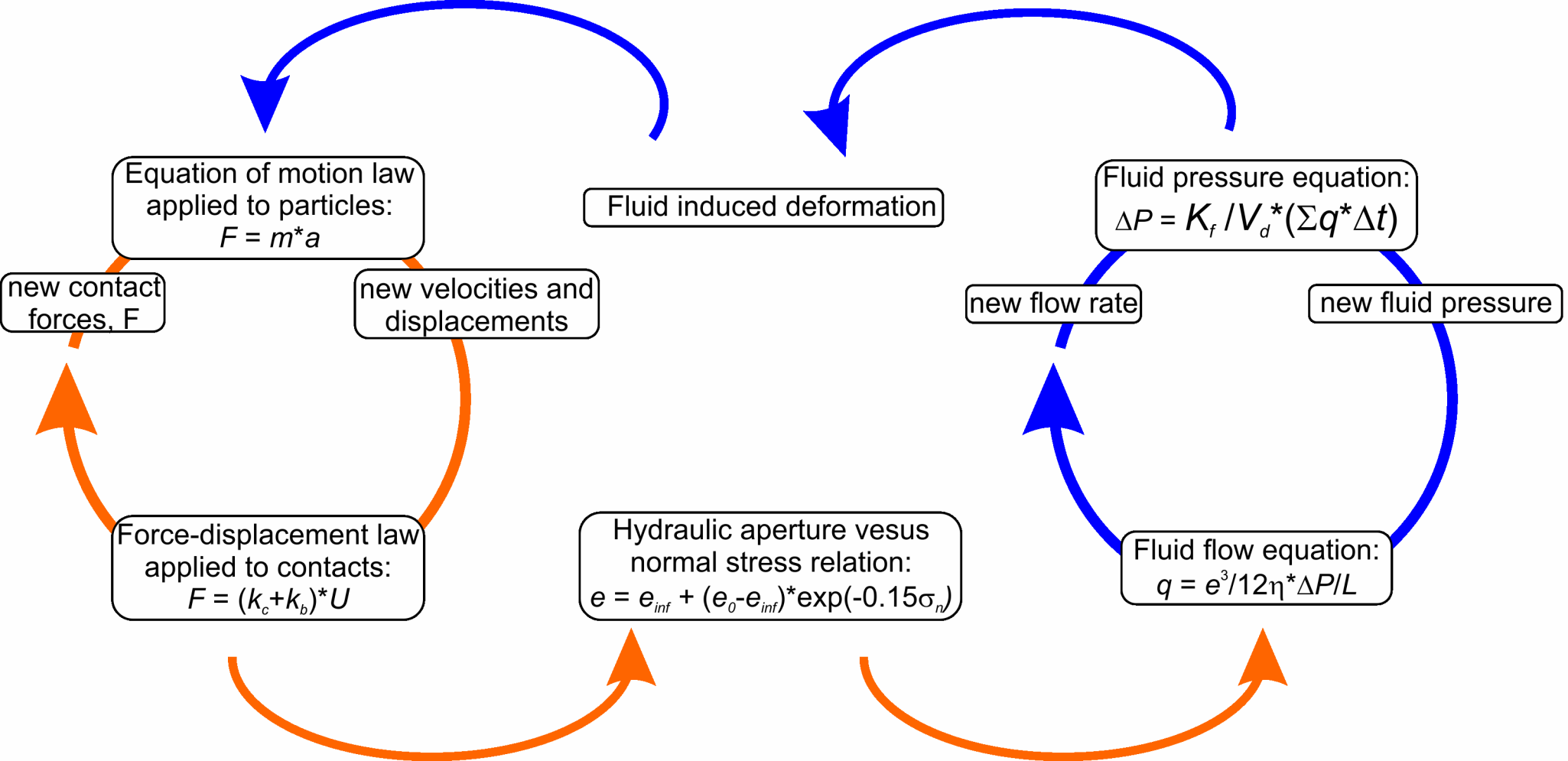
Equation of motion law applied to particles: $F = m*a$
new contact forces, F
new velocities and displacements
Force-displacement law applied to contacts: $F = (k_c+k_b)*U$
Fluid induced deformation
Hydraulic aperture vesus normal stress relation: $e = e_{inf} + (e_0-e_{inf})*\exp(-0.15\sigma_n)$
Fluid pressure equation: $\Delta P = K_f / V_d*(\Sigma q*\Delta t)$
new flow rate
new fluid pressure
Fluid flow equation: $q = e^3/12\eta*\Delta P/L$

10
e_0
1
e_0
0.1
0.01
e (μm)
Foliation
e_{inf}
Intact rock
e_{inf}
$e = e_{inf} + (e_0 - e_{inf})^*\exp(-\alpha^*\sigma_n)$
0
10
20
30
40
50
σ_n (MPa)

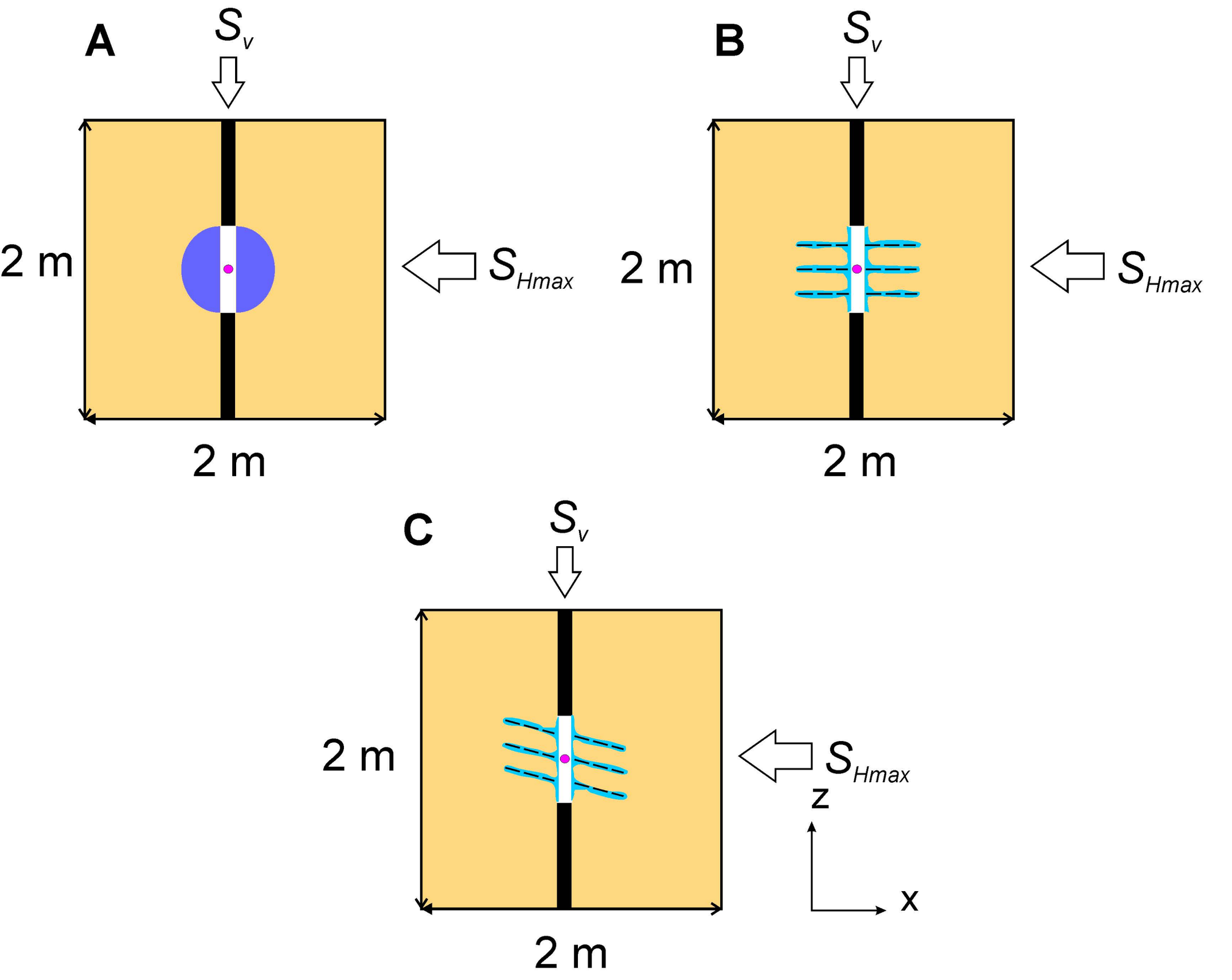
A
S_v
2 m
S_{Hmax}
2 m
B
S_v
2 m
S_{Hmax}
2 m
C
S_v
2 m
S_{Hmax}
z
x
2 m

Cycle 1: Fracture Initiation
Cycle 2: Breakdown
Cycle 3: Refracturing
Injection
Shut-in
Injection
Shut-in
Injection
Shut-in
FBP (A/1)
RFP (A/2)
Interval Pressure (MPa)
Flow rate (l/min)
Cum. number of cracks (1)
Flow time (min)
0
5
10
15
20
25
0
4
8
12
16
20
0
40
80
120
160
200
0
2
4
6
8
10
12
14

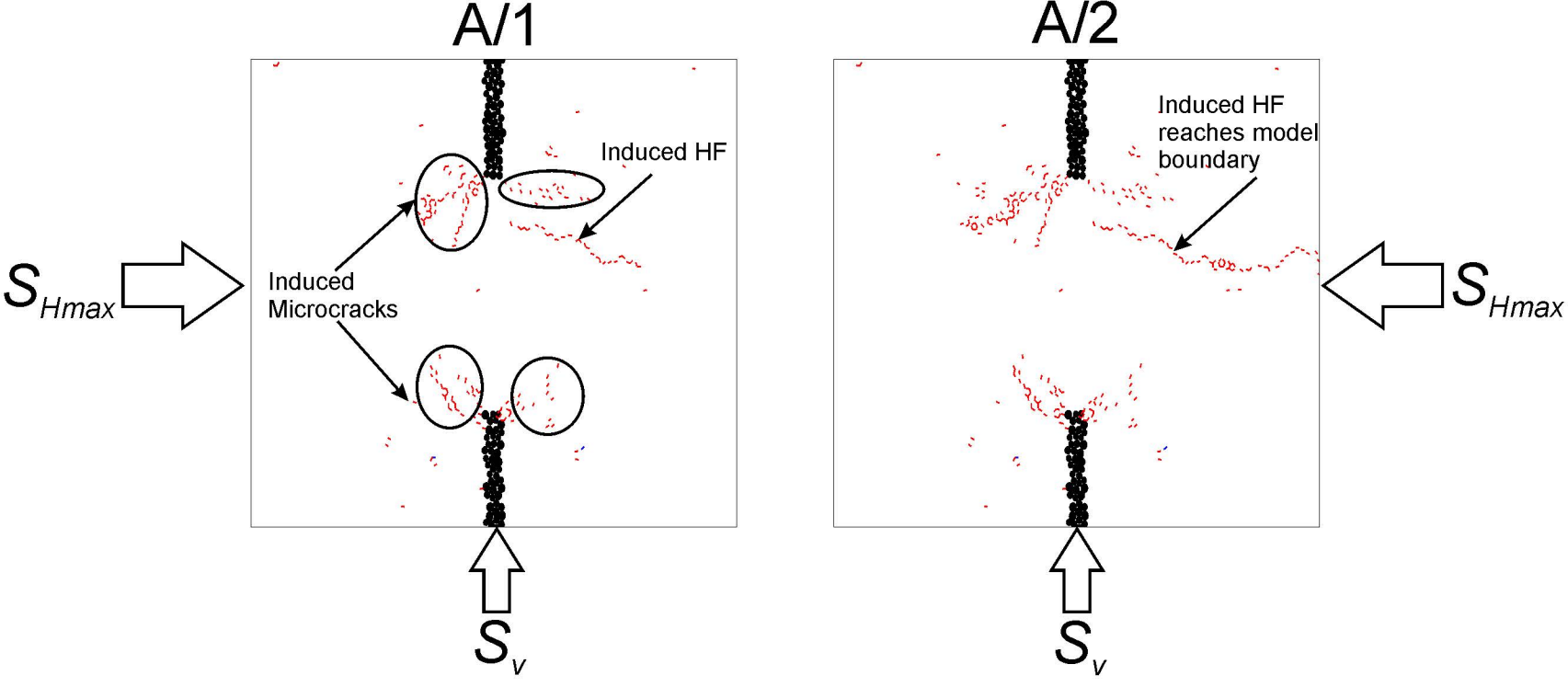
A/1
A/2
Induced HF
Induced
Microcracks
Induced HF
reaches model
boundary
S_{Hmax}
S_{Hmax}
S_v
S_v

Cycle 1: Breakdown

Cycle 2: Refracturing

Injection

Shut-in

Injection

Shut-in

FBP (B/1)

RFP (B/2)

Interval Pressure (MPa)

Flow rate (l/min)

Cum. number of cracks (1)

Flow time (min)

0

5

10

15

20

25

0.0

0.5

1.0

1.5

2.0

0

4

8

12

16

20

0

40

80

120

160

200

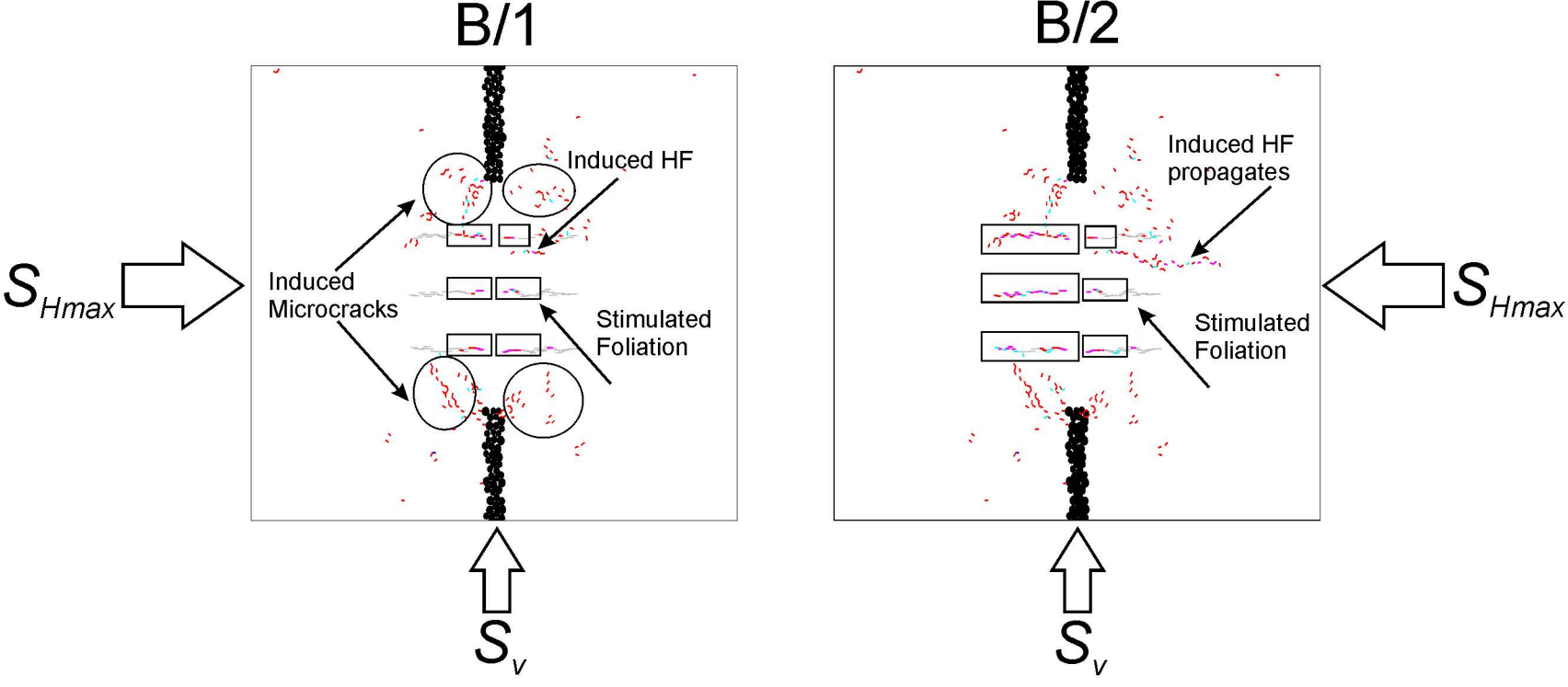
B/1
B/2
Induced HF
Induced
Microcracks
Stimulated
Foliation
Induced HF
propagates
Stimulated
Foliation
S_{Hmax}
S_{Hmax}
S_v
S_v

Cycle 1: Fracture Initiation
Cycle 2: Breakdown
Cycle 3: Refracturing
Injection
Shut-in
Injection
Shut-in
Injection
Shut-in
FBP
(C/1)
RFP
(C/2)
Interval Pressure (MPa)
Flow rate (l/min)
Cum. number of cracks (1)
Flow time (min)
0
6
12
18
24
30
0
4
8
12
16
20
0
40
80
120
160
200
0
1
2
3
4

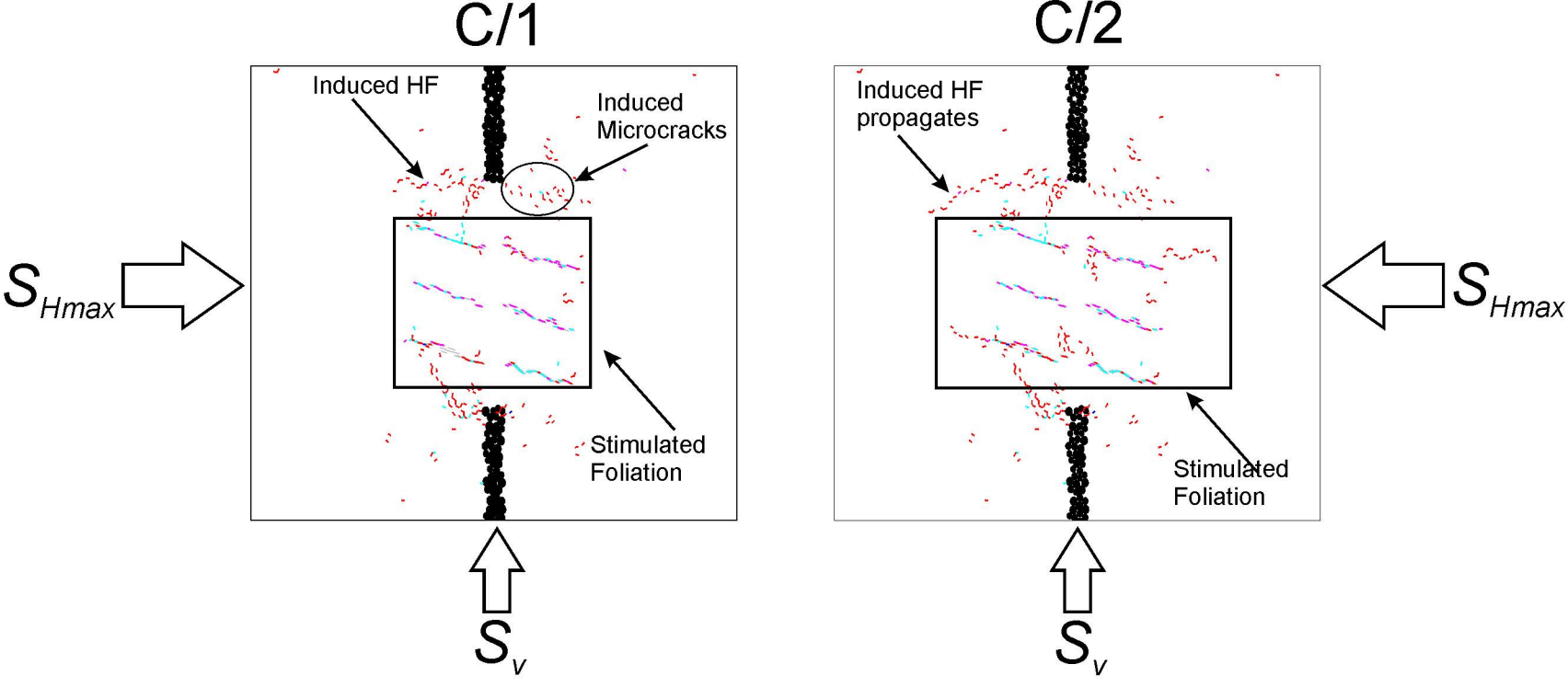
C/1
Induced HF
Induced
Microcracks
Stimulated
Foliation
S_{Hmax}
S_v
C/2
Induced HF
propagates
Stimulated
Foliation
S_{Hmax}
S_v

	Cycle number	Cycle type	Injected Fluid Volume (l)	Flow Back Volume (l)	Peak Pressure (MPa)**	Shut-in Pressure (MPa)	Jacking Pressure (MPa)
Test interval in borehole PAET-26 in Mica Schist* Depth: 540.33 - 541.66 m	1	Breakdown	6.7	4.9	16.5	-	-
	2	Refracturing	6.9	6.5	19.0	**16.4**	-
	3	Refracturing	8.8	8.3	19.3	17.0	-
	4	Refracturing	25.0	7.5	21.7	17.1	-
	5	Jacking	72.0	6.6	21.1	**16.4**	**16.5**
	6	Refracturing	18.6	6.6	20.2	**16.4**	-

* Drilling mud viscosity and density: 10 mPa s, 1060–1160 kg/m^3

** Fracture breakdown pressure (*FBP*), refracturing or reopening pressure (*RFP*) of respective cycles

Particle parameters		Units	Parallel-bond parameters for rock matrix		Units
Particle number	15299	-	Radius multiplier	1	-
Young's modulus	40	GPa	Moment contribution factor	1	-
Normal/shear stiffness ratio	2.5	-	Young's modulus	40	GPa
Coefficient of friction	0.9	-	Normal/shear stiffness ratio	2.5	-
Minimum radius	0.7	mm	Tensile strength	11.5±-1.5	MPa
Max/min radius ratio	1.5	-	Cohesion	26±-2.6	MPa
Ball density	2630	kg/m^3	Angle of internal friction	45	°
Parallel-bond parameters for sealing packers		Units	Parallel-bond parameters for smooth joints		Units
Radius multiplier	1	-	Normal stiffness	300	GPa/m
Moment contribution factor	1	-	Shear stiffness	30	GPa/m
Young's modulus	40	GPa	Friction coefficient	0.9	-
Normal/shear stiffness ratio	2.5	-	Dilation angle	3	°
Tensile strength	20.5	MPa	Tensile strength	3	MPa
Cohesion	35	MPa	Cohesion	0.1	MPa
Angle of internal friction	45	°	Angle of internal friction	30	°

Parameter	Laboratory data (average, min, max)	Simulated data	Units
Young's modulus	36.3, 24.7, 59.7	52.9	GPa
Poisson's ratio	0.25, 0.18, 0.34	0.24	-
Uniaxial compressive strength	65.5, 51.5, 98.8	97.3	MPa
Brazilian tensile strength	4.9; 2.8, 6.4	9.8	MPa

Simulation case	Q (l/min)	V_{inj} (l)	*FBP* (MPa)	*RFP* (MPa)	Generated microcrack failure type (%)*
A – homogeneous rock mass, stimulation by water injection	3.6	14.4	24	21.5	pb_n (100); pb_s (0)
B – horizontally foliated rock mass, stimulation by drilling mud injection	3.6	2.4	17	18.5	pb_n (71); pb_s (0); sj_n (18); sj_s (11)
C – sub-horizontally foliated rock, stimulation by drilling mud injection	3.6	4.8	30	27	pb_n (69); pb_s (0); sj_n (9); sj_s (22)
Field data	3.6–3.8	10^{1}–10^{2**}	16.5	19	-

* failure types: parallel bond, normal (pb_n), parallel bond, normal (pb_s), smooth joint, normal (sj_n) and smooth joint, shear (sj_s)

** injected volume: order of magnitude